

RESEARCH ARTICLE

Hybrid quantum-classical convolutional neural network model for COVID-19 prediction using chest X-ray images

Essam H. Houssein ^{1,*}, Zainab Abohashima², Mohamed Elhoseny^{3,4} and Waleed M. Mohamed¹

¹Faculty of Computers and Information, Minia University, Minia, Egypt; ²Faculty of Computer Science, Nahda University, Beni Suef, Egypt; ³University of Sharjah, Sharjah, United Arab Emirates and ⁴Faculty of Computers and Information, Mansoura University, Egypt

*Corresponding author. E-mail: essam.halim@mu.edu.eg  <http://orcid.org/0000-0002-8127-7233>

Abstract

Despite the great efforts to find an effective way for coronavirus disease 2019 (COVID-19) prediction, the virus nature and mutation represent a critical challenge to diagnose the covered cases. However, developing a model to predict COVID-19 via chest X-ray images with accurate performance is necessary to help in early diagnosis. In this paper, a hybrid quantum-classical convolutional neural network (HQ-CNN) model using random quantum circuits as a base to detect COVID-19 patients with chest X-ray images is presented. A collection of 5445 chest X-ray images, including 1350 COVID-19, 1350 normal, 1345 viral pneumonia, and 1400 bacterial pneumonia images, were used to evaluate the HQ-CNN. The proposed HQ-CNN model has achieved higher performance with an accuracy of 98.6% and a recall of 99% on the first experiment (COVID-19 and normal cases). Besides, it obtained an accuracy of 98.2% and a recall of 99.5% on the second experiment (COVID-19 and viral pneumonia cases). Also, it obtained 98% and 98.8% for accuracy and recall, respectively, on the third dataset (COVID-19 and bacterial pneumonia cases). Lastly, it achieved accuracy and recall of 88.2% and 88.6%, respectively, on the multiclass dataset cases. Moreover, the HQ-CNN model is assessed with the statistical analysis (i.e. Cohen's Kappa and Matthew correlation coefficients). The experimental results revealed that the proposed HQ-CNN model is able to predict the positive COVID-19 cases.

Keywords: COVID-19; medical image classification; deep neural networks; quanvolutional neural networks; quantum computing; image processing

Abbreviations

CNN:	Convolutional Neural Networks	ML:	Machine Learning
TL:	Transfer Learning	COVID-19:	Coronavirus Disease 2019
AI:	Artificial Intelligence	ReLU:	Rectified Linear Unit
RQC:	Random Quantum Circuits	DL:	Deep Learning
QC:	Quantum Computing	Conv layer:	Convolutional layer
Qubit:	Quantum Bit	CXR:	Chest X-ray
		CT:	Computed Tomography

Received: 27 June 2021; Revised: 6 December 2021; Accepted: 12 December 2021

© The Author(s) 2022. Published by Oxford University Press on behalf of the Society for Computational Design and Engineering. This is an Open Access article distributed under the terms of the Creative Commons Attribution License (<http://creativecommons.org/licenses/by/4.0/>), which permits unrestricted reuse, distribution, and reproduction in any medium, provided the original work is properly cited.

ANN:	Artificial Neural Networks
QNN:	Quantum Neural Networks
QCL:	Quantum Computing Learning
NN:	Neural Networks
GAN:	Generative Adversarial Networks
CM:	Confusion Matrix
ROC:	Receiver Operating Characteristic Curve
AUC:	Area Under Curve
MCC:	Matthew Correlation Coefficient

1. Introduction

Recently, coronavirus disease 2019 (COVID-19) has been rapidly spreading in several countries caused by infection of human beings with severe acute respiratory syndrome coronavirus 2 (SARS-CoV-2; Li & Xia, 2020). The ongoing COVID-19 pandemic attacks human health causing respiratory disease and acute kidney injury (Sise et al., 2020). COVID-19 stands for coronavirus disease 2019, which is a new type of coronavirus and falls as a subtype of RNA viruses (Kooraki et al., 2020). The genetic structure of COVID-19 is identical to bat-coronavirus RaTG13, MERS-coronavirus, and SARS-coronavirus by 95%, 50%, and 82%, respectively (Ahmed et al., 2020; Udugama et al., 2020). The first outbreak of the disease was in China at the end of 2019. The most common clinical symptoms of the disease are fever, sore throat, vomiting, nasal congestion, persistent cough, dyspnea, diarrhea, muscle pain, anosmia, fatigue, shortness of breath, chest pain, and chills (Jamil et al., 2020). In March 2020, the World Health Organization reported COVID-19 as a pandemic (Li & Xia, 2020). The most common diagnostic tool used for COVID-19 prediction is a real-time “reverse transcription-polymerase chain reaction” (RT-PCR; Salehi et al., 2020), even though RT-PCR has low recall with the early phases (Xie et al., 2020). Alternative imaging tools [i.e. chest X-ray (CXR) and computed tomography (CT) scans] play an important and critical role in COVID-19 prediction (Li et al., 2020). Radiologists prefer to use the CXR to diagnose chest diseases. The CXR has been used to detect infected COVID-19 cases (Chen et al., 2020). Thus, utilizing the artificial neural networks (NNs) to detect COVID-19 in CXR has become essential.

Recently, many metaheuristic algorithms have been used to overcome the high processing time and accuracy problems (Vania & Lee, 2021), such as modified water cycle algorithm (Tavasoli et al., 2021), arithmetic optimization algorithm (Abualigah et al., 2021a), wild horse optimizer (Naruei & Keynia, 2021), aquila optimizer (Abualigah et al., 2021b), RUNge Kutta optimizer (Ahmadianfar et al., 2021), Archimedes optimization algorithm (Hashim et al., 2020b), Lévy flight distribution (Houssein et al., 2020b), Monarch butterfly optimization (Wang et al., 2019), and Henry gas solubility optimization (Hashim et al., 2019). Since many fields of science need optimization, metaheuristic algorithms have been applied successfully to solve many optimization problems in different domains, such as drug design (Houssein et al., 2020a), maximizing lifetime of wireless sensor networks (Ahmed et al., 2019), bioinformatics (Hashim et al., 2020a), information feedback (Zhang et al., 2020), Job-shop scheduling problem (Gao et al., 2020), and feature selection (Neggaz et al., 2020). In general speaking, several metaheuristic algorithms have been applied to present the COVID-19 disease classification and prediction, e.g. the marine predators algorithm (MPA; Abdel-Basset et al., 2020) and Salm swarm algorithm (Al-qaness et al., 2020; Chattopadhyay et al., 2021) golden ratio optimizer.

The convolutional neural networks (CNNs) are one of the most widespread deep learning (DL) models in image classifi-

cation (Miller & Brown, 2018) and image segmentation (Vania et al., 2019). Various works of the COVID-19 prediction of cases using CNN structure have been proposed; these works are presented in detail in Section 2. The authors (Chowdhury et al., 2020) proposed deep CNN models to pretrain their model using transfer learning (TL) to discuss the leverage of artificial intelligence (AI) for COVID-19 classification using CXR images. The computational power of classical ANN especially cannot learn large training data with low cost (Lundervold & Lundervold, 2019). It is not especially capable of generating more kernels (kernel estimation) with high-dimensional features (Havlíček et al., 2019; Schuld & Killoran, 2019). Effortlessly, quantum computing (QC) is capable of performing complex kernels in n -dimensional space.

On the other hand, the QC field has proven its significant role in intractable problems with classical counterparts via quantum supremacy (Boixo et al., 2018; Arute et al., 2019) and with the upgrowth of the concept of QC and its improvements in the machine learning (ML) field (i.e. learning capacity, run time, and learning efficiency; Dunjko & Briegel, 2018). QC has also demonstrated a remarkable influence in the ML field on near-term quantum computers (Killoran et al., 2019). Lately, quantum neural network (QNN) approaches have been proposed (Farhi & Neven, 2018; Jeswal & Chakraverty, 2019). According to the best of our knowledge, the start point of QNN was in 1995. Kak (Kak, 1995) introduced NN concepts in the QC world. This study focuses on the hybrid classical-quantum approach. The authors (Henderson et al., 2020) presented a new quantum convolutional layer within CNN based on quantum circuits to estimate kernel in high dimensionality. In a similar work (Havlíček et al., 2019), the authors proposed a quantum kernel algorithm of support vector machines to estimate kernel with a quantum circuit and to deal with huge features by estimating kernel in n -dimensionality space. The authors (Mitarai et al., 2018) proposed a new hybrid method called QC learning (QCL) based on a quantum circuit. QCL works with large datasets for clustering, regression, and classification tasks. Recently, the quantum circuit is used with CNN for COVID-19 classification using CT images (Amin et al., 2021) and speech recognition (Yang et al., 2021).

Therefore, the motivation behind this work is to combine the advantage of the quantum convolutional layer with CNN and CXR images as a pivot tool and the cheapest diagnostic technique of COVID-19 to produce a new proposed hybrid quantum-classical convolutional neural network (HQ-CNN) model. This model aims to improve the performance of CNN to detect coronavirus cases in early phases. The HQ-CNN model is measured with two angle encoding gates and a different number of shots. The better results have been achieved by the Ry angle gate and 500 shots. The proposed HQ-CNN model achieved higher performance with an accuracy of 98.6% and 82.6% on binary and multiclass datasets, respectively. The experimental results show the ability of the proposed HQ-CNN model to classify positive COVID-19 cases. The restrictions of the HQ-CNN model are highlighted in Section 5.4.

The main contributions of this work are as follows:

1. A new hybrid CNN model combined with a quantum circuit for image processing called HQ-CNN model for coronavirus disease 2019 prediction-based CXR images is proposed.
2. HQ-CNN model is evaluated on binary and multiclass datasets with confirmed coronavirus disease 2019 cases.
3. An exhaustive and comparative experimental discussion is presented in terms of accuracy, average accuracy, recall, specificity, precision, F1-measure, receiver operating characteristic (ROC)-area under curve (AUC), Kappa score, and

confusion matrix (CM) to evaluate the performance of the proposed HQ-CNN model.

The remainder of this paper is organized as follows: Section 2 gives an overview of recent COVID-19 classification based on the CNN with CXR and CT images and shows a comparative performance of previous works. Background about the concept of QC (quantum bits and quantum gates) and CNN are presented in Section 3. The hybrid proposed HQ-CNN model is introduced in detail in Section 4. Section 5 presents the used datasets, performance measures, the experimental results, and discussion of the hybrid HQ-CNN model. Finally, the conclusion of this work and future research are delineated in Section 6.

2. Literature Review

This section provides various works of COVID-19 classification based on CNN. Related works are divided into studies based on CXR images and CT scans.

The authors presented a new model using ensemble learning and DL called EDL-COVID for COVID-19 patient classification using CXR images (Tang et al., 2021). They proposed a weighted average ensembling for various ML techniques. EDL-COVID model obtained an accuracy of 95%. In Johri et al. (2021), this study introduced a new multiclass ML model to classify COVID-19, viral and bacterial pneumonia, and normal patients via CXR images. The used dataset is split into training, validation, and testing images. The proposed model achieved accuracies of 92.4%, 88.24%, and 87.13% for training, validation, and testing, respectively. The authors presented a new self-supervised learning technique using supersample decomposition from unlabeled CXR images, named 4S-DT (Abbas et al., 2021). They presented a generic coarse-to-fine TL technique for incrementally improving the quality of transformation from large-scale images. Deep local features are extracted using the autoencoder technique from each sample in a superlarge dataset. In the downstream training phase, they offer a downstream class decomposition layer to handle any abnormalities in the data distribution and simplify the local structure. The 4S-DT model obtained an accuracy of 97.54%.

In Apostolopoulos and Mpesiana (2020), the authors proposed a CNN model based on TL to extract meaningful biomarkers of coronavirus patients. This model utilized various CNN architectures (i.e. VGG19, Xception, and MobileNetV2) for classifying COVID-19 images. The tenfold cross-validation is used to evaluate the proposed model. The results are reported with 96.78% accuracy (2-class), 94.72% accuracy (3-class), 98.66% recall, and 96.46% specificity for the MobileNet V2 model. A patch-based technique utilizing statistical analysis with ResNet18 and fully convolutional-DenseNet103 architectures is presented in Oh et al. (2020). Due to the lack of CXR images for COVID-19, this technique is used with a small dataset to classify COVID-19 patients. Moreover, the proposed technique has achieved an accuracy of 88.9% and a precision of 83.4%. In another study (Das et al., 2020), a deep CNN model is introduced to detect positive patients of COVID-19, called Truncated InceptionNet. The inceptionNetV3 is modified with the Truncated model to deal with limited datasets of COVID-19 to reduce overfitting. Besides, 162 COVID-19 confirmed cases are added to 6 datasets. The proposed model is evaluated with different datasets to test its ability for predicting positive cases of COVID-19 of each dataset. This model achieved 99.9% accuracy for the fifth dataset with 162 COVID-19, 1583 normal, and 4280 pneumonia.

The DarkNet technique is presented for COVID-19 classification using CXR images in Ozturk et al. (2020). This model is predicted COVID-19 cases without using feature extractor algorithms. This model is applied as a classifier for YOLO object detection. This model is used with binary and multiclass COVID-19 classification. The DarkNet model achieved 98.08%, 95.13%, 95.30%, and 96.51% for accuracy, recall, specificity, and F1-measure, respectively. Besides, the model achieved an accuracy of 87.02% for a multiclass dataset. The DarkNet model consists of 17 Conv layers and 1164434 parameters. In another work (Islam et al., 2020), a hybrid CNN-LSTM model is presented using CNN and long short-term memory to detect COVID-19 cases. The CNN is utilized for feature extraction and LSTM for the classification of images. The CNN-LSTM model has achieved higher results with 99.4%, 99.3%, 99.2%, 99.9%, and 99.9% for accuracy, recall, specificity, AUC score, and F1-measure, respectively. Also, the ROC-AUC curve and CM are provided to evaluate the CNN-LSTM model. This model has 20 layers.

In Khan et al. (2020), a deep CNN based on the Xception model is introduced, called CoroNet. The proposed model utilized an ImageNet dataset for the pretrained process. This model is evaluated on binary and multiclass datasets with 284 COVID-19 images. The proposed CoroNet model accomplished an accuracy of 99%, 95%, and 89.6% for binary, three-class, and four-class datasets. The overall accuracy achieved is 89.6%. In this study (Brunese et al., 2020), the VGG16 architecture is used with TL for COVID-19 classification using CXR images. The two models are proposed to classify between (COVID-19 vs. healthy) and (COVID-19 vs. pulmonary). The first model achieved 96% of accuracy and recall 98% of specificity, and 94% of F1-measure.

The second model accomplished 98%, 87%, 94%, and 89% for accuracy, recall, specificity, and F1-measure, respectively.

On the other side, a hybrid gravitational search algorithm (GSA)-DenseNet121 DL model is presented using a gravitational search optimizer (Ezzat et al., 2020). The GSA is used for the hyperparameters tuning of the DenseNet121 model. Random copying is performed to balance the used dataset. The proposed model achieved an accuracy of 98.3%. In a similar work (Sahlol et al., 2020), a hybrid CNN's technique is proposed using a swarm-based optimizer for COVID-19 classification. The hybrid technique is combined among inception model, Marine Predators, and fractional-order calculus algorithms. The Inception CNN model is used for feature extraction. The MPA is applied to reduce extractor features by the selection of meaningful features. The proposed technique Inception Fractional-order Marine Predators Algorithm (IFM) is improved using the fractional-order calculus algorithm. The proposed IFM technique achieved an accuracy of 98.7% and an F1-score of 98.2% for the first dataset. The results of 99.6% for accuracy and 99% for F1-score are obtained for the second dataset.

A new approach (Toraman et al., 2020) is proposed utilizing capsule network and CXR images for COVID-19 case detection called the CapsNet model. This model is evaluated on binary and multiclass datasets. This model has used 1050 CXR images for COVID-19, normal, and pneumonia classes. For binary dataset, The CapsNet model has accomplished 97.24%, 97.42%, 97.04%, 97.08%, and 97.24% for accuracy, recall, specificity, precision, and F1-measure, respectively. Also, the results 84.22% for accuracy, 84.22% for recall, 91.79% for specificity, 84.61% for precision, and 84.21% for F1-measure are achieved for the multiclass dataset. In another separate study (Marques et al., 2020), a novel system using the EfficientNet model to diagnose COVID-19 patients. The EfficientNet has used a tenfold cross-validation technique

Table 1: Comparison between the existing related studies.

Work	Images	Type	Method	Data	AC. (%)	Train time (s)	No. of params (m)
(Johri et al., 2021)	560 COVID-19, 591 viral, 2116 bacterial, 1058 normal	CXR	ML model	Imbalanced	87.13	-	-
(Abbas et al., 2021)	-	CXR	4S-DT	Imbalanced	97.54	-	-
(Apostolopoulos & Mpesiana, 2020)	224 COVID-19, 714 pneumonia, 504 normal	CXR	MobileNetV2	Imbalanced	96.78	-	-
(Oh et al., 2020)	180 COVID-19, 191 normal, 131 others	CXR	ResNet18	Imbalanced	88.9	-	-
(Das et al., 2020)	162 COVID-19	CXR	CNN	Imbalanced	99.9	-	2.1
(Ozturk et al., 2020)	125 COVID-19, 500 normal	CXR	DarkNet	Imbalanced	98.08	-	1.16
(Islam et al., 2020)	1525 COVID-19, 1525 normal, 1525 pneumonia	CXR	CNN + LSTM	Balanced	99.4	18 372.0	-
(Khan et al., 2020)	284 COVID-19, 330 bacterial, 310 normal, 327 viral	CXR	Xception	Balanced	89.6	-	33.96
(Brunese et al., 2020)	250 COVID-19, 2753 pneumonia, 3520 normal	CXR	VGG16	Imbalanced	96	-	-
(Ezzat et al., 2020)	99 COVID-19, 207 non-COVID-19	CXR	DenseNet121 + GSA	Balanced	98.3	-	-
(Sahlot et al., 2020)	200 COVID-19, 1675 non-COVID-19	CXR	Inception + FO-MPA	Imbalanced	98.7	-	-
(Sahlot et al., 2020)	219 COVID-19, 1341 non-COVID-19	CXR	Inception + FO-MPA	Imbalanced	99.6	-	-
(Toraman et al., 2020)	1050 COVID-19, 1050 normal	CXR	Capsule Network	Balanced	97.24	-	-
(Toraman et al., 2020)	1050 COVID-19, 1050 normal, 1050 pneumonia	CXR	Capsule Network	Balanced	84.22	-	-
(Marques et al., 2020)	504 COVID-19, 500 normal	CXR	EfficientNet	Balanced	99.62	284 976	17.91
(Marques et al., 2020)	504 COVID-19, 500 normal, 504 pneumonia	CXR	EfficientNet	Balanced	96.70	402 588	17.91
(Ucar & Korkmaz, 2020)	76 COVID-19, 4290 pneumonia, 1583 normal	CXR	COVIDagnosis-Net	Imbalanced	98.3	2277.6	-
(Hemdan et al., 2020)	25 COVID-19, 25 normal	CXR	VGG19	Balanced	90	2641	143
(El Asnaoui & Chawki, 2020)	231 COVID-19, 4273 pneumonia, 1583 normal	CT and CXR	InceptionResNetV2	Imbalanced	92.18	79 184.28	-
(Wang et al., 2021a)	84 COVID-19, 281 community-acquired pneumonia, 293 secondary pulmonary tuberculosis, and 306 healthy	CT	CCSHNet	Balanced	-	-	-
(Xu et al., 2020)	219 COVID-19, 175 normal, 224 pneumonia	CT	3D-DL	Balanced	86.7	-	-
(Singh et al., 2020)	73 COVID-19	CT	CNN + MODE	-	92	-	-
(Wu et al., 2020)	368 COVID-19, 127 pneumonia	CT	ResNet50	Imbalanced	76	-	-
(Jaiswal et al., 2020)	1262 COVID-19, 1230 non-COVID-19	CT	DenseNet201	Balanced	97	-	-

for binary and multiclass classification with 1508 total number of CXR images. This model reported binary class results 99.62% for accuracy, 99.63% for recall, 99.64% for precision, and 99.62% for F1-score. The model achieved 96.70%, 96.69%, 97.59%, and 97.11% for accuracy, recall, precision, and F1-score, respectively, with multiclass classification.

The authors (Wang et al., 2021a) designed a new AI model for COVID-19 classification from CT images using TL, called CCSHNet. They used six pretrained models (i.e. DenseNet201, ResNet101, and VGG19) to extract features of CT images. Also, they proposed a new selection method to select the best two models and then combine the extracted features using “the discriminant correlation analysis” technique. They reported that the CSSHNet model outperformed 12 other methods. The CSSHNet model obtained a micro-averaged F1 of 97.04%. In Wang et al. (2021b), the authors introduced a new model based on the PatchShuffle method, called PSSPNN. The PSSPNN model classifies between proposed novel PSSPNN model for the classification of COVID-19, healthy, community-captured pneumonia, and secondary pulmonary tuberculosis cases. They presented five improvements in their model: first, they presented the “n-Conv stochastic pooling module” using stochastic pooling. Second, they proposed a new stochastic pooling NN (SPNN) based on the VGG-16 model. Third, the PatchShuffle method is combined with SPNN to add the concept of the regularization term. Fourth, to avoid overfitting, the 16-way is used to enhance data augmentation. Lastly, “gradient-weighted class activation mapping” is utilized to interpret the PSSPNN model.

In Xu et al. (2020), a 3D CNN is introduced based on the location-attention model to distinguish COVID-19 patients using CT images. This model achieved a classification accuracy of 86.7%. In another study with CT images (Singh et al., 2020), the CNN model is proposed with multi-objective differential evolution for tuning hyperparameters of CNN. The results are reported with 0.92% accuracy and 0.90% for recall, specificity, and F1-measure. The ResNet50 model (Wu et al., 2020) is used with multiview images for the classification of COVID-19 patients with chest CT scans. The proposed model achieved an AUC of 81.9%, a recall of 81.8%, an accuracy of 76%, and a specificity of 61.5%. In Jaiswal et al. (2020), a DL technique is proposed using DenseNet-201 model and TL. The proposed technique is applied with learned weights of the ImageNet dataset to extract features. It has achieved an accuracy of 97% compared to Resnet152V2, VGG16 models. Besides, it obtained an ROC-AUC score of 0.97%.

In El Asnaoui and Chawki (2020), the authors present a comparative work of the CNN architectures (i.e. Inception.ResNet.V2, VGG16, VGG19, Resnet50, Inception.V3, MobileNet.V2, and DenseNet201). They used L2-regularizers and weight decay to avoid overfitting in various architectures. The architectures are used CT and CXR images. The Inception.Resnet.V2 obtained higher accuracy of 92.18%.

2.1. The strengths and limitations of literature review

The previous studies faced inconsistency issues due to a variety of methods, images, and a variety of data. A brief comparison

of the previous research has been presented in terms of the applied methods, images, data, and classification performance (as shown in Table 1). Since chest CXR and CT scans are the second tools to diagnose and detect the COVID-19 pandemic, the classification of COVID-19 has become a hot area of research. The researchers collected datasets from several resources to train and test the models as shown in Table 1.

The authors in Apostolopoulos and Mpesiana (2020) reported that the COVID-19 detection is rapid and low cost. Some of the defects were mentioned in this study. (i) The study used a small number of positive COVID-19 cases. (ii) The used pneumonia images are older recorded cases before suspected COVID-19. Also, the proposed model in Das et al. (2020) proved its superiority for COVID-19 diagnosis. The proposed Truncated InceptionNet model has 2.1 million trainable parameters in contrast the InceptionNet V3 has 21.7 million trainable parameters. The main advantage of Ozturk et al. (2020) is an assessment of the DarkNet model by radiologists and the limitation of this work is the limited images number. In Islam et al. (2020), the size of the dataset is small. The performance of the proposed model is not compared with radiologists. It cannot distinguish other CXR views (i.e. anterior-posterior).

The proposed model (Toraman et al., 2020) has a fewer number of layers (four Conv layers). With huge images, capsule networks need a lot of computational resources machines, which increases processing time. As a result, the study relied on images of small size. The CCSHNet model is unable to process heterogeneous data. Also, this study uses a limited dataset. Finally, the CCSHNet model is not compared with clinical validation (Wang et al., 2021a).

From the previous studies, the training phase needs a lot of computational time. Therefore, COVID-19 prediction must become a more fast model to save training time. To identify COVID-19 cases, significant research has been conducted in the literature review. Because of the restricted data availability and high-cost DL training in the previous studies, the primary goal of this study is to build a new model to overcome the current high-cost DL training with higher performance. Table 1 shows a comparison between the existing related studies in terms of the used image number (Images), type of the used images (Type), the used method (Method), balanced data (Data), accuracy (AC), training time in seconds (Train time), and the number of parameters in million [No. of params (m)].

3. Preliminaries

This section presents QC concepts like the quantum bit, quantum gates, and the architecture of CNN. If the reader is familiar with these concepts, then he/she may skip this subsection.

3.1. Quantum computing

QC relies on postulates and characteristics of quantum mechanics (i.e. quantum bits, interference, superposition, and entanglement) for information processing. QC gives us the ability to solve complex problems better and faster than classical computing (Aïmeur et al., 2006; Dunjko et al., 2016). Quantum bit (qubit) is the small unit to process information in a quantum computer like the bit in classical computing. A qubit can also be in one-state, zero-state, or both states at the same time, known as linear superposition. The qubit is a state vector in Hilbert space.

$$|\psi\rangle = \begin{pmatrix} \theta \\ \delta \end{pmatrix} = \theta|0\rangle + \delta|1\rangle, \quad (1)$$

where θ and δ are the probability amplitudes that are represented by complex numbers and $|\theta^2| + |\delta^2| = 1$.

From the postulates of quantum mechanics, any unitary transformation (unitary matrix) is a quantum gate. For this matrix (U) to be unitary, the following condition must be verified:

$$UU^\dagger = U^\dagger U = I, \quad (2)$$

where U^\dagger is the conjugate transpose of a matrix U and I is an identity matrix. Quantum gates can be classified based on numbers of qubits: one-qubit gates, two-qubit gates, and multiple-qubit gates (Nielsen & Chuang, 2002; Kaye et al., 2007). First, the most popular and widely used gate in one-qubit gates is a Hadamard gate or square-root of the NOT gate. The Hadamard gate is used to create a superposition state between two qubits. Pauli gates also are one-qubit gates. Second, two-qubits gates work on 4×4 unitary matrices, e.g. controlled NOT and swap gate. Lastly, multiple-qubit gates work on multiple qubits as $2^n \times 2^n$ unitary matrices such as Toffoli and swap gates. Table 2 shows quantum gates with circuit representation, unitary matrix, the number of qubits, and the operation of the gate.

3.2. Convolutional neural networks

CNN (LeCun et al., 1989) inspired by convolution operation to produce a convolutional (Conv) layer. The basic architecture of CNN is similar to a multilayer perceptron starts with the input image and sequence of hidden layers to predict labels over the output layer. The layers of CNN are explained in detail in Section 4. The CNN plays a critical role in computer vision applications such as image classification (Das et al., 2020), image segmentation (Liu et al., 2019), object detection (Li et al., 2019), and signal processing (Vrysis et al., 2020). Various models have been developed based on the concepts of CNN as ResNet50 and VGG-19.

4. Proposed HQ-CNN Model

The proposed HQ-CNN model aims to enhance the CNN performance for medical images and to predict COVID-19 cases. The main idea of the HQ-CNN model is based on hybrid computation (Bergholm et al., 2018). The proposed model consists of two parts: first, the quantum part is utilized in the quantum Conv layer, which is proposed by the authors (Henderson et al., 2020). Second, the classical part with CNN structure. As shown in Fig. 1, the HQ-CNN model has one quantum Conv layer, three Conv layers followed by the rectified linear unit activation function, and two max-pooling layers, followed by two fully connected (FC) layers.

The layers of the model are presented in detail in the following steps.

4.1. Quantum convolutional layer

The proposed HQ-CNN model has used quantum convolution that is presented by the authors (Henderson et al., 2020). The main idea of convolutional layers is used to preprocess the local patches of an image rather than preprocess the entire original image. This concept is developed further in the context of quantum circuits. The main difference between quantum convolution and classical convolution is that a quantum circuit may generate complicated kernels whose processing may be classically stubborn (Henderson et al., 2020; Amin et al., 2021). Quantum convolution works as small random quantum circuits (RQCs) to calculate convolution operation, using RQCs to match near-term quantum devices and noisy intermediate-scale quantum

Table 2: Summarizes standard QC gates.

Gate	Notation	Matrix	Qbit	Use
Hadamard		$\frac{1}{\sqrt{2}} \begin{pmatrix} 1 & 1 \\ 1 & -1 \end{pmatrix}$	1	Create superposition state between two quantum bits.
Pauli-X		$\begin{pmatrix} 0 & 1 \\ 1 & 0 \end{pmatrix}$	1	Flip quantum bit from one state to another.
Pauli-Y		$\begin{pmatrix} 0 & -i \\ i & 0 \end{pmatrix}$	1	Make π -rotation for quantum bit around the Y-axis.
Pauli-Z		$\begin{pmatrix} 1 & 0 \\ 0 & -1 \end{pmatrix}$	1	Make π -rotation for quantum bit around the Z-axis.
Swap		$\begin{pmatrix} 1 & 0 & 0 & 0 \\ 0 & 0 & 1 & 0 \\ 0 & 1 & 0 & 0 \\ 0 & 0 & 0 & 1 \end{pmatrix}$	2	Swap two quantum bits states.
Toffoli		$\begin{pmatrix} 1 & 0 & 0 & 0 & 0 & 0 & 0 & 0 \\ 0 & 1 & 0 & 0 & 0 & 0 & 0 & 0 \\ 0 & 0 & 1 & 0 & 0 & 0 & 0 & 0 \\ 0 & 0 & 0 & 1 & 0 & 0 & 0 & 0 \\ 0 & 0 & 0 & 0 & 1 & 0 & 0 & 0 \\ 0 & 0 & 0 & 0 & 0 & 1 & 0 & 0 \\ 0 & 0 & 0 & 0 & 0 & 0 & 0 & 1 \\ 0 & 0 & 0 & 0 & 0 & 0 & 1 & 0 \end{pmatrix}$	3	Controlled-Controlled NOT (CC Not) gate. Flip target quantum bit if both control two quantum bits equal one.

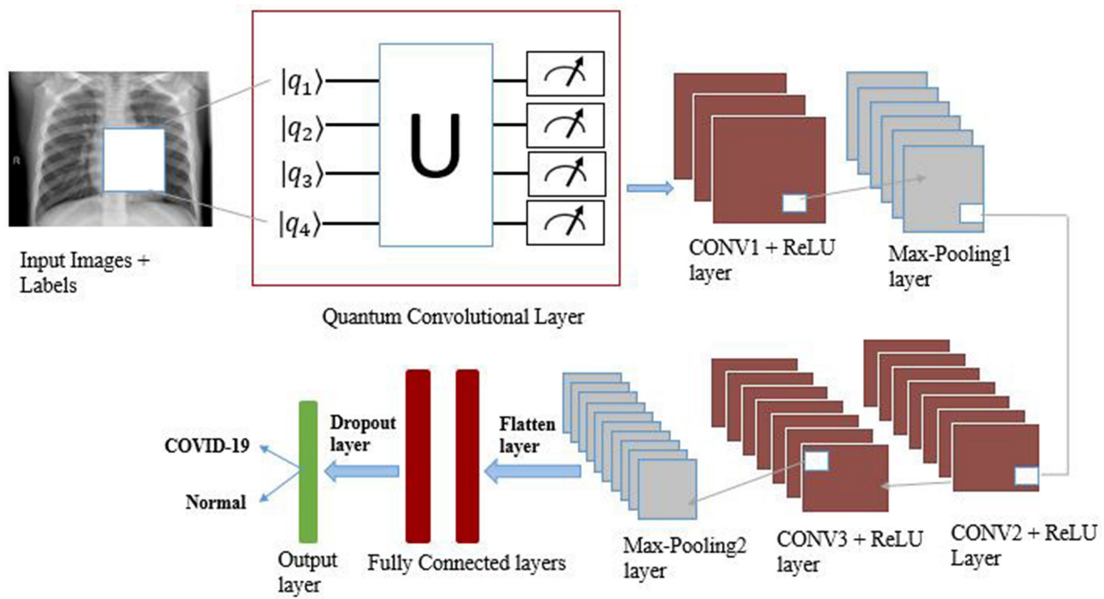


Figure 1: Block diagram for proposed HQ-CNN model.

hardware. The quantum pennylane device is initialized to mimic the four-qubit device. The RQC works with (2×2) small squares of an input image. Each (2×2) square of the image is encoded into a quantum state by the RY gate. The encoding process is repeated in different patches of the image. This process is compatible with the classical convolution process with a kernel

size of (2×2) and stride is equal to 2. The RQC consists of four layers (qubits) compatible with (2×2) squares. The expectation values are calculated. These values are mapped into four channels of output (single-pixel), as drawn in Fig. 4. The quantum convolution layer consists of three phases, namely encoding, RQC, and decoding (as shown in Fig. 2).

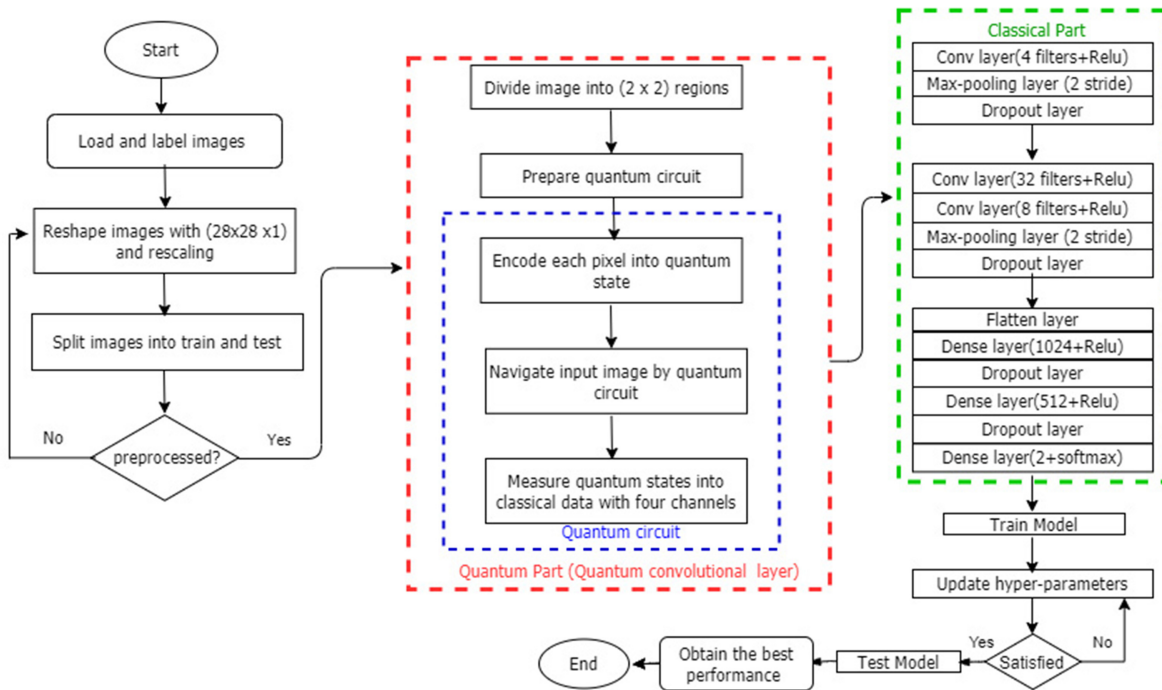


Figure 2: Flowchart for proposed HQ-CNN model.

4.1.1. Encoding

Up till now, encoding data to quantum is a challenge in quantum machine learning (Houssein et al., 2022). Several encoding methods have been discussed in Lloyd et al. (2020). In this work, angle encoding is used to transform input data into rotation angles of quantum states. The angle rotation gates are the simplest encoding methods to access data in a quantum circuit. In this study, due to needing the single quantum gate for each entry to encode data, these gates are corresponding to encode classical pixel data to a quantum state. Rotation matrices are rotation operators of Pauli matrices in the form of exponential around the X, Y, and Z axes (as seen in Table 1). The three rotation gates Rx, Ry, and Rz are a single quantum bit rotation via angle α around the X, Y, and Z axes, respectively.

The RY and RX rotation gates can be represented by the following equations:

$$R_x(\alpha) = \begin{pmatrix} \cos\left(\frac{\alpha}{2}\right) & -i \sin\left(\frac{\alpha}{2}\right) \\ -i \sin\left(\frac{\alpha}{2}\right) & \cos\left(\frac{\alpha}{2}\right) \end{pmatrix} \quad (3)$$

$$R_y(\alpha) = \begin{pmatrix} \cos\left(\frac{\alpha}{2}\right) & -\sin\left(\frac{\alpha}{2}\right) \\ \sin\left(\frac{\alpha}{2}\right) & \cos\left(\frac{\alpha}{2}\right) \end{pmatrix}. \quad (4)$$

4.1.2. Random quantum circuits

A quantum circuit is a series of quantum unitary operations (or gates) and measurements connected via wires (Qubits). Just like the classical Conv layer, the quantum Conv layer composed of quantum kernels applies to the input image. The main idea of quantum convolution utilizes RQCs to split input images into small local locations to extract meaningful features. The advantage of the quantum circuit in quantum convolution is that it works with a few quantum bits and shallow depth of quantum circuits.

4.1.3. Measurement

The measurement phase is also known as the decoding phase. Decoding is measuring quantum data to transform into a classical form. Pauli matrices can be used as measurement methods (Takeuchi et al., 2019). In the HQ-CNN model, the Pauli-Z gate is used for the decoding phase (as seen in Table 2).

4.2. Convolutional layer

Conv layer is the pivotal and significant layer in the feature extraction part of CNN. This layer performs convolution operation on input features with kernels to extract invariant and informative features from images as convoluted features map to the next layer. Convolution operation computes dot products between small local locations of the input image and kernels (Zhang et al., 2016; Ozturk et al., 2020).

$$(F * K)(i, j) = \sum_m \sum_n K(m, n) F(i - m, j - n), \quad (5)$$

where $*$ is the convolution operation to produce a convoluted feature map, F is the input feature, and K is the kernel or filter. The Conv layer is followed by the ReLU function transformation, which adds activation values into the model network. The function returns 0 for all negative values and returns the maximum value for all positive values. The ReLU function can be defined by the following formula:

$$\text{ReLU}(x) = \max(0, x), \quad (6)$$

where x is an input value.

4.3. Max-pooling layer

The Max-pooling layer is used to reduce computational learning by selecting the most important and valuable features. Convoluted feature maps have been divided into small regions based on the stride number. The max-pooling idea has taken the

Table 3: Shows the summary of the HQ-CNN model.

Layer	Type	Units	Kernel size	Input size	No. of parameters
1	Quantum Conv	4	2 × 2	(28 × 28 × 1)	-
2	Conv2D	16	2 × 2	(14 × 14 × 4)	136
3	MaxPooling2D	-	2 × 2	(14 × 14 × 4)	-
4	Conv2D	16	2 × 2	(7 × 7 × 4)	528
5	Conv2D	32	2 × 2	(7 × 7 × 32)	2080
6	MaxPooling2D	-	2 × 2	(7 × 7 × 8)	-
7	FC1	300	-	(288)	86 700
8	FC2	100	-	(300)	30 100
9	Output	2	-	(100)	202

Table 4: Summarizes the five experiments that are used in this work.

Experiment	COVID-19	Normal	Viral	Bacterial	Train	Test	Total
E1	1350	1350	-	-	945 COVID-19, 945 normal	405 COVID-19, 405 normal	2700
E2	1350	-	1345	-	945 COVID-19, 942 viral	405 COVID-19, 403 viral	2695
E3	1350	-	-	1400	945 COVID-19, 980 bacterial	405 COVID-19, 420 bacterial	2750
E4	1350	1350	1345	1400	945 COVID-19, 945 normal, 942 viral, 980 bacterial	405 COVID-19, 405 normal, 403 viral, 420 bacterial	5445
E5	3616	4000	-	-	2509 COVID-19, 2822 normal	1107 COVID-19, 1178 normal	7616

maximum value of each small location to produce pooled feature maps. Before the classification part, flatten layer is used to link two parts in CNN by converting the max-pooled feature map into a one-dimensional array.

4.4. Fully connected layer

The FC layer is the second part of the CNN structure. The FC layers perform the classification process after the flatten layer by applying weights to predict classes. The dropout layer is used after the FC layer to reduce the overfitting of the model (as shown in Fig. 2).

Figure 2 illustrates the flowchart of the HQ-CNN model: The proposed HQ-CNN model has nine layers, one quantum Conv layer, three classical Conv layers with ReLU function, two max-pooling layers, and two FC layers with ReLU function, and one output layer is applied with a softmax activation function. The quantum Conv layer consists of three parts; the encoding part with the RY rotation gate, RQCs, and decoding with the Pauli-Z gate. The three classical Conv layers are used with 2D CNN and are combined with the max-pooling layer. Each max-pooling layer is performed with a (2×2) kernel size and the stride equal to 2, followed by a dropout layer with a 0.2 dropout rate. The two FC layers are applied with 300 and 100 neurons for the first and second layers, respectively. The total parameters for the HQ-CNN model are 119 645. Table 3 shows the summary layers of the proposed HQ-CNN model.

5. Experimental Results and Discussion

This section introduces the used images dataset, the performance measures to evaluate the HQ-CNN model, and the analysis and discussion of experimental results.

5.1. Dataset

The used dataset in this study is collected by the research team from Qatar, Malaysia, and Pakistan in collaboration with

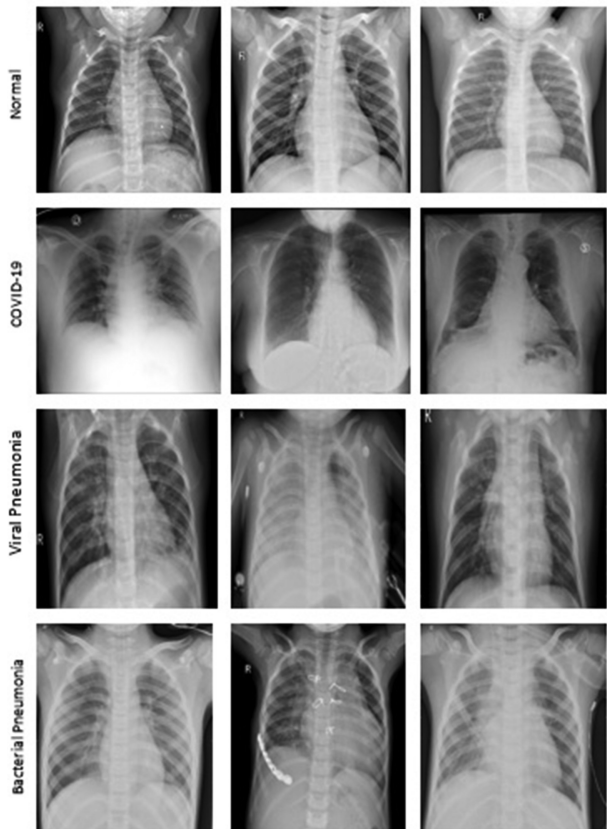


Figure 3: Samples of used images.

the medical doctors (Chowdhury et al., 2020). This CXR image dataset is released in phases: The first phase is released with 219 COVID-19, 1345 viral pneumonia, and 1341 normal CXR images. The second phase is released with 1200 COVID-19, 1345 viral pneumonia, and 1341 normal CXR images. The third phase

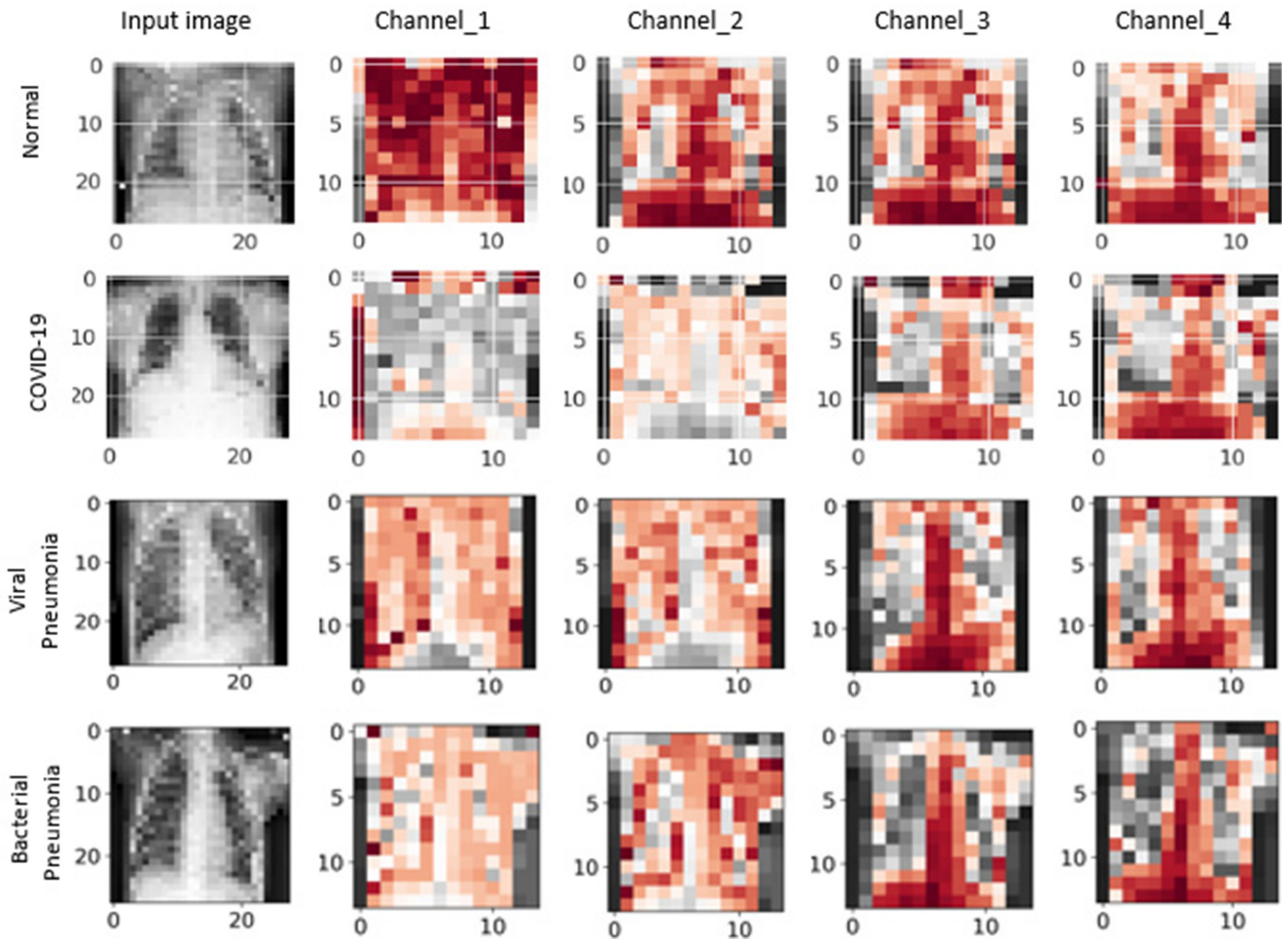


Figure 4: Samples of normal, COVID-19, viral, and bacterial images are preprocessed by RQCs.

is released with 3616 COVID-19, 10 192 normal, 1345 viral pneumonia, and 6012 lung opacity images. For this study, only 1350 COVID-19, 1350 normal, and 1345 viral pneumonia CXR images are adapted for the balanced dataset. To classify COVID-19, and bacterial pneumonia images, the 1400 images of bacterial pneumonia are adapted from Kermany et al. (2018). The CXR images are divided into five experiments to investigate the ability of the proposed HQ-CNN model to detect COVID-19 cases. Table 4 summarizes the used CXR experiments in this work. Figure 3 shows samples from the used images.

5.2. Performance measures

The most common measures for evaluating classification models are CM with metrics like accuracy, specificity (or true-negative rate), recall (true-positive rate), precision, and F1-measure. The metrics are computed in terms of TP, TN, FP, and FN. These terms can be defined as follows:

1. True Positives (TP): The proposed HQ-CNN model correctly predicts COVID-19 cases and labelled as COVID-19.
2. True Negatives (TN): The proposed HQ-CNN model correctly predicts normal cases and labelled as normal.
3. False Positive (FP): The proposed HQ-CNN model incorrectly predicts normal cases and labelled as normal.

4. False Negatives (FN): The proposed HQ-CNN model incorrectly predicts COVID-19 cases and labelled as COVID-19.

$$\text{Accuracy} = \frac{\text{TP} + \text{TN}}{\text{TP} + \text{TN} + \text{FP} + \text{FN}} \quad (7)$$

$$\text{Specificity} = \frac{\text{TN}}{\text{TN} + \text{FP}} \quad (8)$$

$$\text{Recall} = \frac{\text{TP}}{\text{TP} + \text{FN}} \quad (9)$$

$$\text{Precision} = \frac{\text{TP}}{\text{TP} + \text{FP}} \quad (10)$$

$$\text{F-measure} = \frac{2 \times \text{Recall} \times \text{Precision}}{\text{Recall} + \text{Precision}} \quad (11)$$

$$\text{FPR} = \frac{\text{FP}}{\text{FP} + \text{TN}} \quad (12)$$

ROC curve identified as ROC-AUC is the method to measure the ability of the classifier to predict the right labels. The ROC is a curve between the true-positive rate (recall) and the false-positive rate (1 – recall). Cohen's Kappa score is a statistic value

Table 5: The performance of the HQ-CNN model with rotation gates and number of shots in E1.

Rotation gate	Shots	AC. (%)	Sn. (%)	Sp. (%)	Pr. (%)	F1-measure(%)	Kappa score(%)
RY	500	98.1	96.7	99.5	99.4	98.1	96.2
		97.6	95.8	99.5	99.4	97.6	95.3
RY	1000	97.6	95.8	99.5	99.4	97.6	95.3
		97.9	96.2	99.5	99.4	97.8	95.8

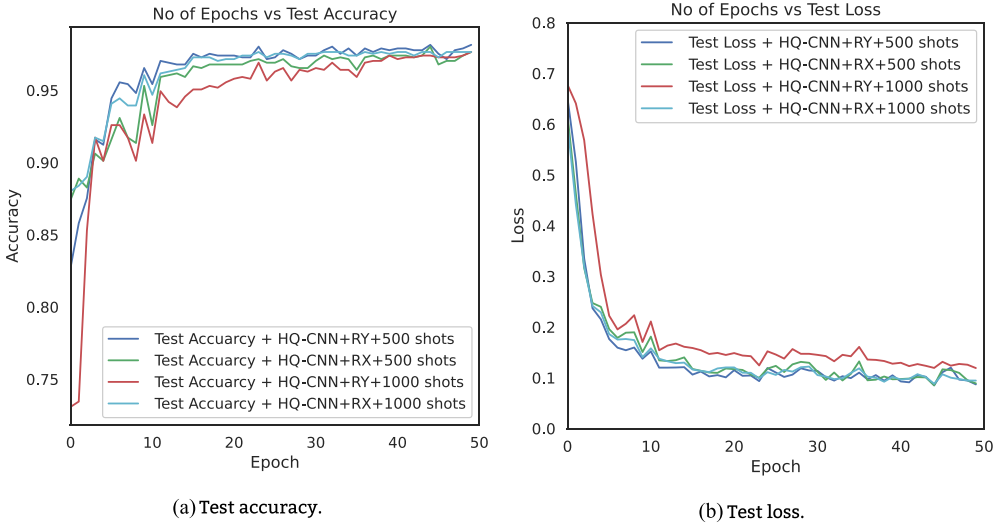


Figure 5: Visualization of the learning curve for both (a) test accuracy and (b) test loss of E1 with 50 epochs.

that calculates the consistency of the HQ-CNN prediction model. It compares the expected and actual results of the HQ-CNN model. That value is in the range of 0–1 (McHugh, 2012). Matthew correlation coefficient (MCC) is statistically derived from the CM. MCC measures the classification performance quality (Chicco & Jurman, 2020; Chicco et al., 2021).

5.3. Experimental results

This subsection presents experimental setup (Section 5.3.1) and the experimental results. The experimental results of HQ-CNN are divided into five parts to measure the ability of the proposed HQ-CNN model for the classification of COVID-19 patients. (i) The classification results of the HQ-CNN model between normal and COVID-19 cases (Section 5.3.2). (ii) The experimental results of the HQ-CNN model between COVID-19 and viral pneumonia patients (Section 5.3.3). (iii) The results of the HQ-CNN model between COVID-19 and bacterial pneumonia patients (Section 5.3.4). (iv) The performance of the HQ-CNN model for a multiclass dataset among normal, COVID-19, and pneumonia patients (Section 5.3.5). (v) The classification results of the HQ-CNN model between normal and COVID-19 cases with increasing the number of images (Section 5.3.6).

5.3.1. Experimental setup

Experimental results have been implemented on the Google Co-laboratory platform by using PennyLane 0.17.0, TensorFlow 2.2.0, and Python 3.7. PennyLane is a cross-platform Python library for hybrid quantum-classical computation (Bergholm et al., 2018). In this work, the images were split into 70% and 30% for train and test images, respectively. RQC works with (2×2) small

squares of an input image. Each (2×2) square of the image is encoded into a quantum state by the RY gate. The decoding of the quantum state into classical produces four new channels of a small square. Figure 4 shows samples of normal, COVID-19, viral, and bacterial images, which are examined by the RQC. The first column shows the input image with (28×28) size and divided by 250. The quantum Conv layer assigns a feature map to four channels. The quantum Conv layer is used only as a pre-processing layer to CXR images. The train and test phases will be completed on quantum preprocessed data with CNN layers. The HQ-CNN model is optimized with the Adam algorithm with a learning rate of 0.0001. The proposed HQ-CNN model results are compared with the classical CNN. The performance of HQ-CNN model is evaluated with measure metrics as represented in equations (7), (8), (9), (10), (11), Cohen's Kappa score, and the ROC-AUC curve.

At the beginning of the evaluation, the proposed model is evaluated with RY and RX gates to encode data into RQC. The RY and RX gates were used with a different number of shots (500 and 1000); shots represent circuit evaluations to measure the expectation values of qubit state. As to be noted from Table 5, the RY gate (500 shots) achieved higher results 98.1%, 96.7%, 99.5%, 99.4%, 98.1%, and 96.2% for accuracy, recall, specificity, precision, F1-measure, and Kappa score, respectively.

Figure 5a depicts the test accuracy of the proposed HQ-CNN model. As shown in Fig. 5b, the test loss curve of the HQ-CNN model with RY (500 shots) continues to reduce until the end of the test phase. The test loss with RY (1000 shots) is 0.087%. Figure 6 shows the CM for RY and RX with a different number of shots. The RY (500 shots) has predicted the highest number of positive cases of COVID-19 (403 of 405 cases). To sum up, the RY

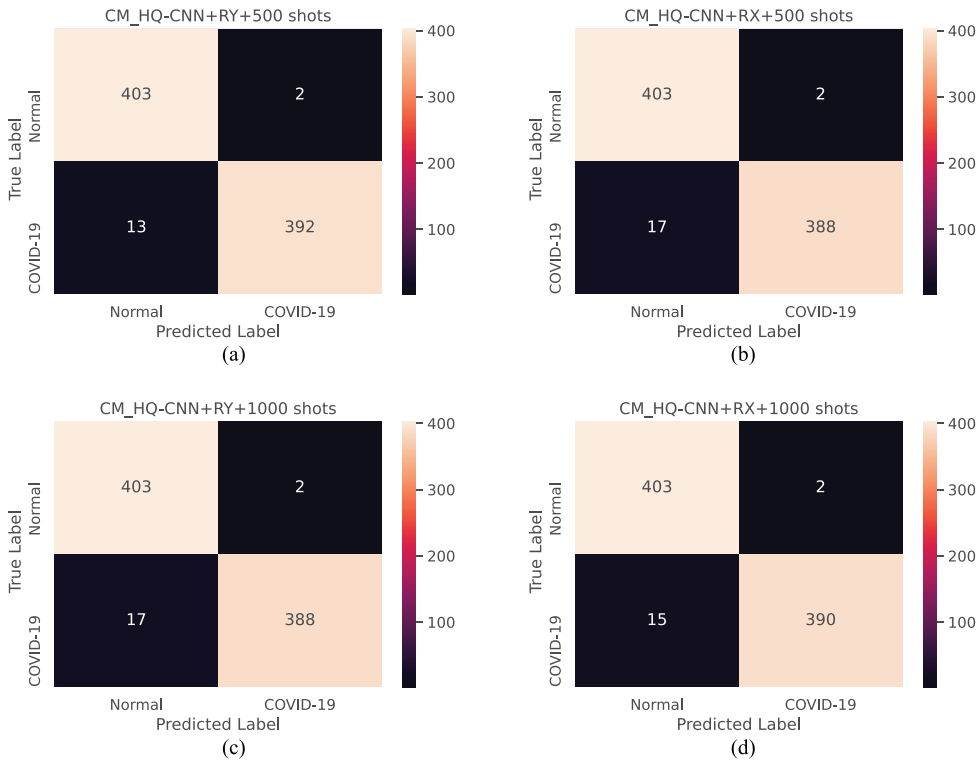


Figure 6: The CM of the proposed HQ-CNN with RY and RX gates. (a) RY(500 shots), (b) RX(500 shots), (c) RY (1000 shots), and (d) RX (1000 shots).

Table 6: Comparison of classification performance between proposed HQ-CNN and CNN models on the five experimental results.

Experiment	Model	AC. (%)	Avg.AC. (%)	Re. (%)	Sp. (%)	Pr. (%)	F1-measure(%)	Kappa score(%)	MCC(%)
E1	HQ-CNN	98.6	98.2	99	98.2	98.2	98.6	97.2	97.2
	CNN	98.5	98.5	99.5	97.5	97.5	99.5	97	97
E2	HQ-CNN	98.2	97.8	99.5	97	97	98.2	96.5	96.5
	CNN	98.2	98.3	99.2	97.2	97.3	98.2	96.5	96.5
E3	HQ-CNN	98	97.9	98.8	97.2	97.4	98.1	96.1	96.1
	CNN	97.9	98.2	98	97.7	97.8	97.9	95.1	95.8
E4	HQ-CNN	82.6	82.5	82.6	–	82.8	82.3	76.8	77.1
	CNN	87.8	87.4	87.8	–	88.1	87.7	83.8	83.9
E5	HQ-CNN	93.3	92.8	93.3	93.3	93.6	93.5	86.6	86.6
	CNN	93.7	94.1	91.2	96.3	96.4	93.7	87.4	87.6

gate achieved better results compared to the RX gate. The experimental results will be completed with an encoding angle (RY gate) and 500 shots.

5.3.2. Experiment 1: normal and COVID-19 cases

As shown in Table 6, the performance of the hybrid proposed HQ-CNN model of experiment 1 (E1) outperforms CNN. The HQ-CNN model predicted COVID-19 and normal cases with 98.6% accuracy, 99% recall, 98.2% specificity, 98.2% precision, and 98.6% F1-measure. The HQ-CNN and CNN models scored the highest AUC of the ROC curve with 0.99% (near to 1), as shown in Fig. 13a. As shown in Fig. 7, the CM of the HQ-CNN model, among 405 COVID-19 images, shows that 7 patients are misclassified by the HQ-CNN model. From a total of 504 normal cases, 4 cases are misclassified by the HQ-CNN model. Meanwhile, 10 cases of COVID-19 cases are misclassified by the CNN model. Figure 8 shows the learning curve of test accuracy and loss with/without quantum Conv layer.

5.3.3. Experiment 2: COVID-19 and viral pneumonia cases

Here, Table 6 reports the results of the HQ-CNN and CNN models of experiment 2 (E2). The HQ-CNN model achieved 98.2%, 99.5%, 97%, and 98.2% for accuracy, recall, precision, and specificity, and F1-measure, respectively. From Fig. 13b, the HQ-CNN model achieved the ROC-AUC score of 99.7% (near to 1). The HQ-CNN model distinguished between COVID-19 and viral pneumonia with higher efficiency. The CM of E2 is shown in Fig. 9. From a total of 405 COVID-19 cases, 12 cases are misclassified by the HQ-CNN model. Among 405 viral pneumonia images, 2 patients are misclassified by the HQ-CNN model. Figure 10 illustrates the test accuracy and loss learning curves with and without the quantum Conv layer.

5.3.4. Experiment 3: COVID-19 and bacterial pneumonia cases

In experiment 3 (E3), the HQ-CNN model achieved 98%, 98.8%, 97.2%, 97.4%, and 98.1% for accuracy, recall, and specificity, precision, and F1-measure, respectively, as noted in Table 6.

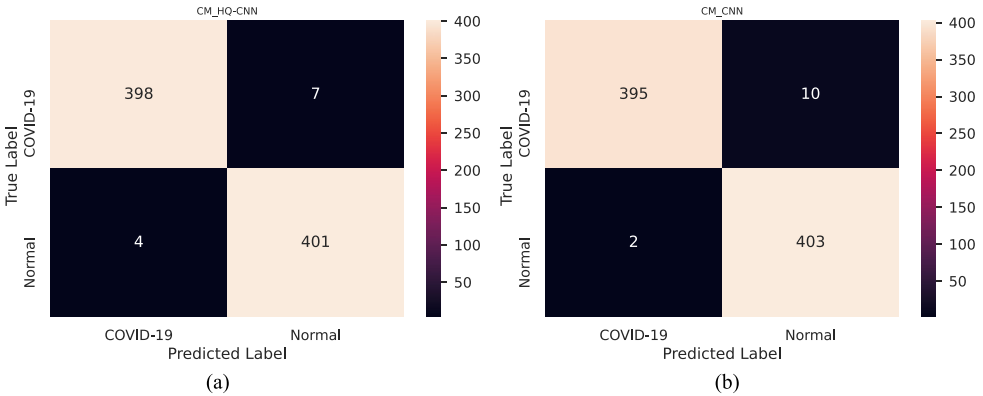


Figure 7: The CM of E1 (a) HQ-CNN and (b) CNN.

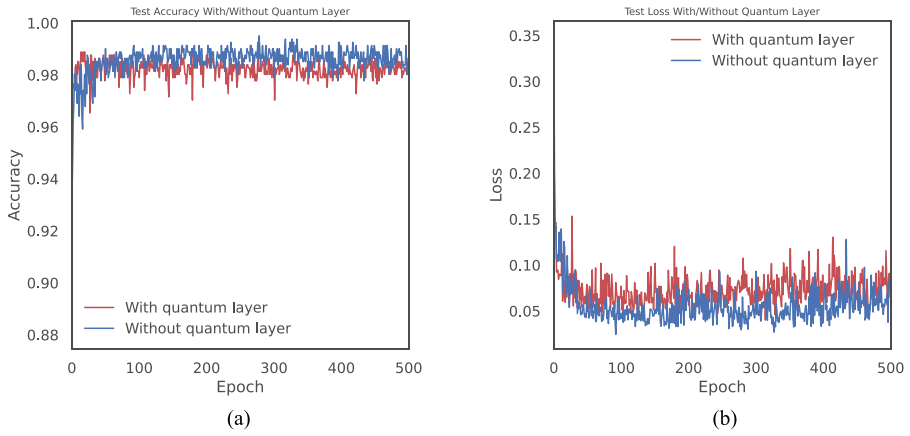


Figure 8: Visualization of the learning curve for both (a) test accuracy and (b) test loss of E1 with 500 epochs.

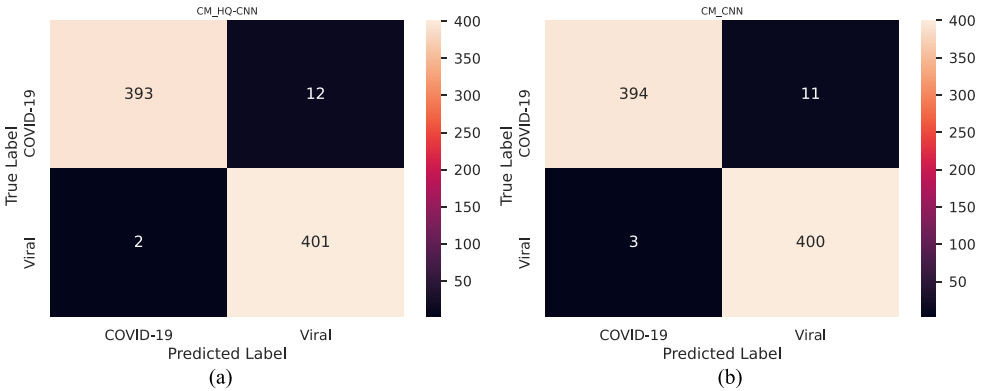


Figure 9: The CM of E2 (a) HQ-CNN and (b) CNN.

From Fig. 13c, the proposed HQ-CNN model achieved the ROC-AUC score of 99.2%. The HQ-CNN model distinguished between COVID-19 and bacterial pneumonia with higher efficiency. The CM of E3 is shown in Fig. 11. The HQ-CNN model misclassifies 11 COVID-19 cases out of 405 cases. Among 405 pneumonia images, 5 patients are misclassified by the HQ-CNN model. Besides, the test accuracy and loss learning curves with and without the quantum Conv layer are depicted in Fig. 12.

5.3.5. Experiment 4: normal, COVID-19, and pneumonia cases

To further evaluate the HQ-CNN model, the dataset is combined with normal, COVID-19, viral pneumonia, and bacterial pneumonia images for evaluating HQ-CNN performance (E4). Table 6 presents the classification results of the HQ-CNN and CNN models on the multiclass dataset. The results are evaluated with 82.6%, 82.6%, 82.8%, and 82.3% for accuracy, recall, precision, and F1-measure, respectively. Besides, The CM of E4 is shown

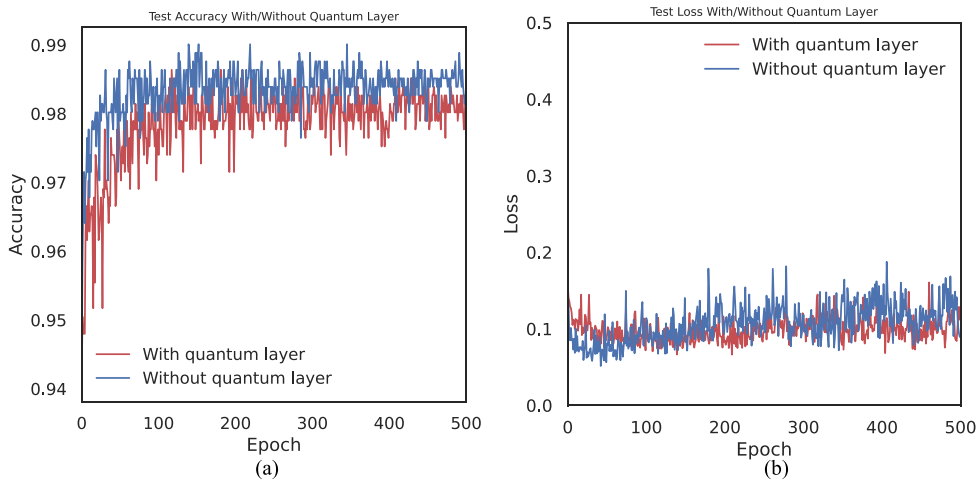


Figure 10: Visualization of the learning curve for both (a) test accuracy and (b) test loss of E2 with 500 epochs.

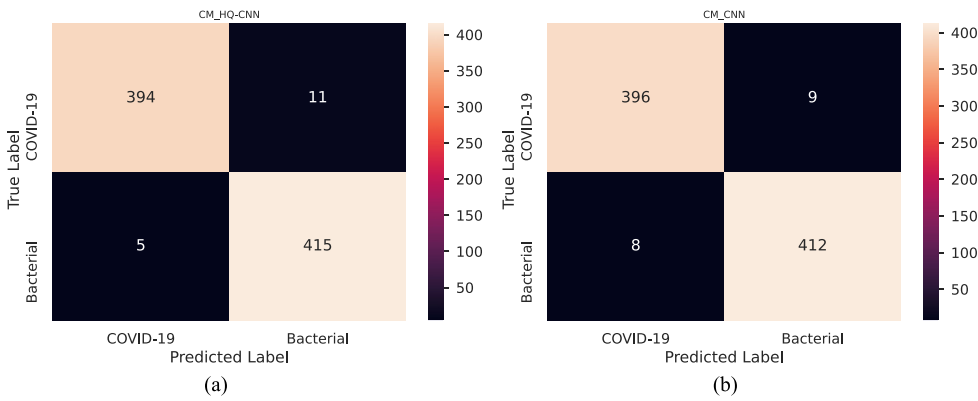


Figure 11: The CM of E3 (a) HQ-CNN and (b) CNN.

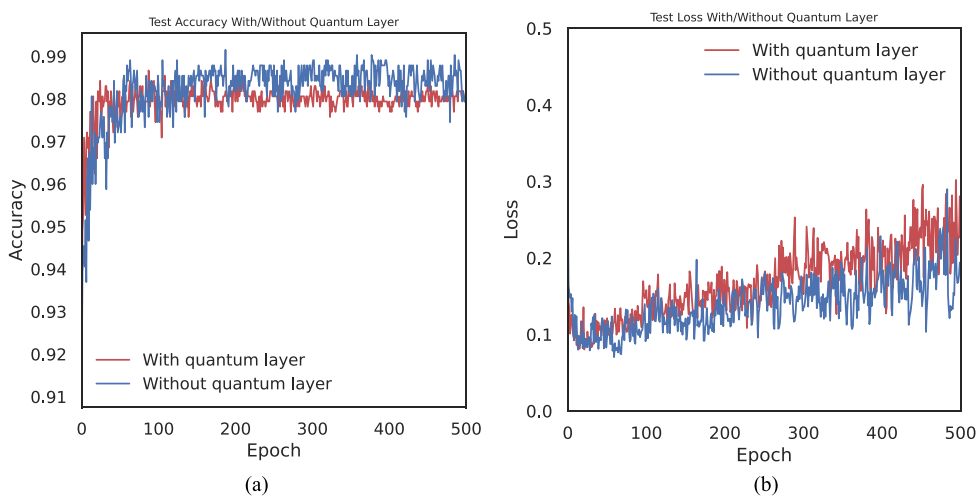


Figure 12: Visualization of the learning curve for both (a) test accuracy and (b) test loss for E3 with 500 epochs.

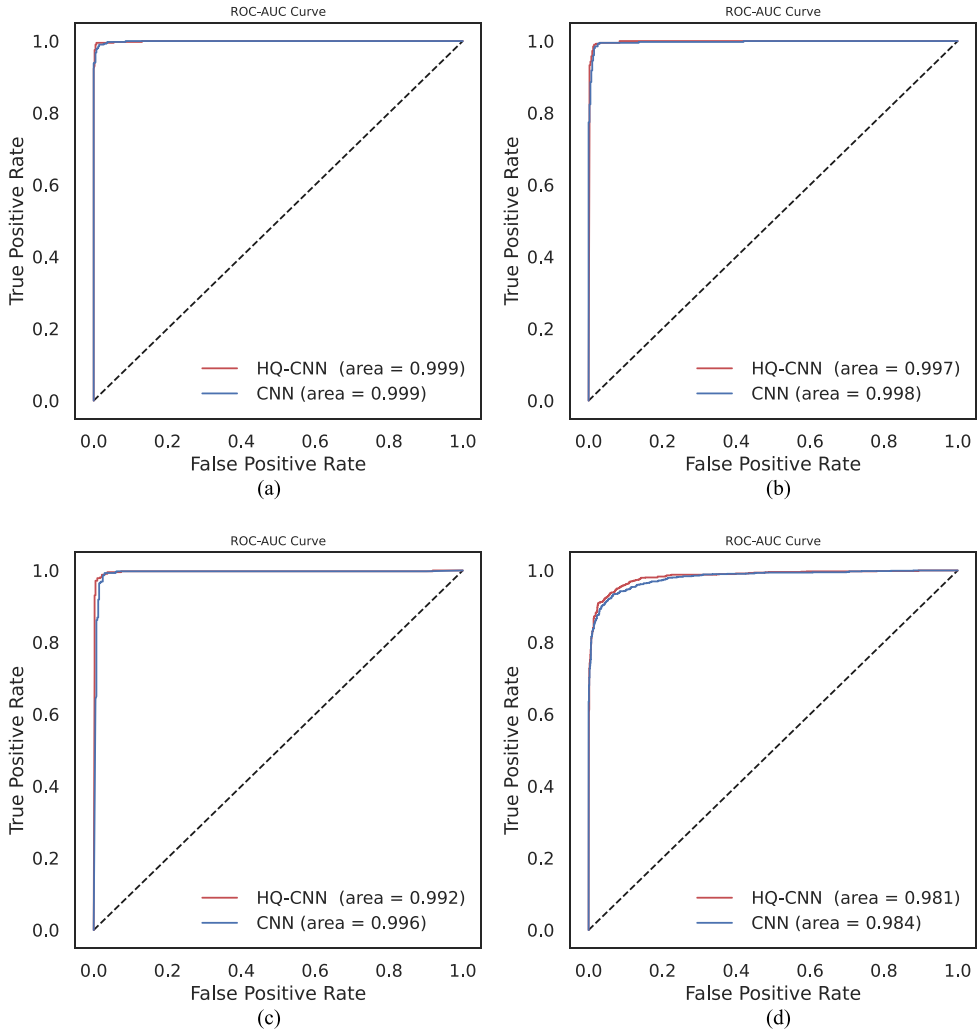


Figure 13: The ROC-AUC curve of HQ-CNN and CNN models: (a) E1, (b) E2, (c) E3, and (d) E5.

in Fig. 14. Figure 15 shows the learning curve of test accuracy and loss with/without quantum Conv layer.

5.3.6. Experiment 5: normal and COVID-19 cases

We used this experiment (E5) to allow for further validation of the HQ-CNN model with more COVID-19 CXR images. As shown in Table 6, the HQ-CNN model predicted COVID-19 and normal cases with 93.3% accuracy, 93.3% recall, 93.3% specificity, 93.6% precision, and 93.5% F1-measure, respectively. The HQ-CNN and CNN models scored the highest AUC of the ROC curve with 98.1% and 98.4%, respectively, as shown in Fig. 13d. As shown in Fig. 16, the CM of the HQ-CNN model, among 1107 COVID-19 images, shows that 74 patients are misclassified by the HQ-CNN model. From a total of 1178 normal cases, 78 cases are misclassified by the HQ-CNN model. Meanwhile, 40 cases of COVID-19 cases are misclassified by the CNN model. Figure 17 shows the learning curve of test accuracy and loss with/without quantum Conv layer.

5.4. Discussion

By analysing the experimental results, the CNN and RQC have been shown to have considerable effects on COVID-19 detection using X-ray images. The proposed approach could accurately

identify COVID-19, viral pneumonia, and bacterial pneumonia, as well as normal instances. When opposed to classical computing, QC provides a more general structure for DL. The objective function optimization is improved by QC. It shortens the time required for DL training (Ciliberto et al., 2018; Dunjko & Briegel, 2018), and this is accomplished in our model . The main idea of convolutional layers is to use local regions of an image rather than processing the entire original image with a global function. This concept is developed further in the context of quantum circuits. The main difference between quantum convolution and classical convolution is that a quantum circuit may generate complicated kernels whose processing may be classically stubborn.

The HQ-CNN model is compared to CXR existing studies, as shown in Table 7. From E1, E2, and E3 (Table 6), the HQ-CNN model outperforms some previous studies with CXR images in terms of accuracy, recall, and F1-measure. The Truncated InceptionNet and CNN + LSTM models outperform the HQ-CNN model in terms of accuracy. The Truncated InceptionNet achieved 99.9% accuracy for one dataset, but the overall accuracy was 98.77%. The Truncated InceptionNet is based on a large InceptionNetV3 model. The CNN + LSTM has 20 layers, including 12 Conv layers. The HQ-CNN model achieved better results with nine layers, including four Conv layers (one quantum layer

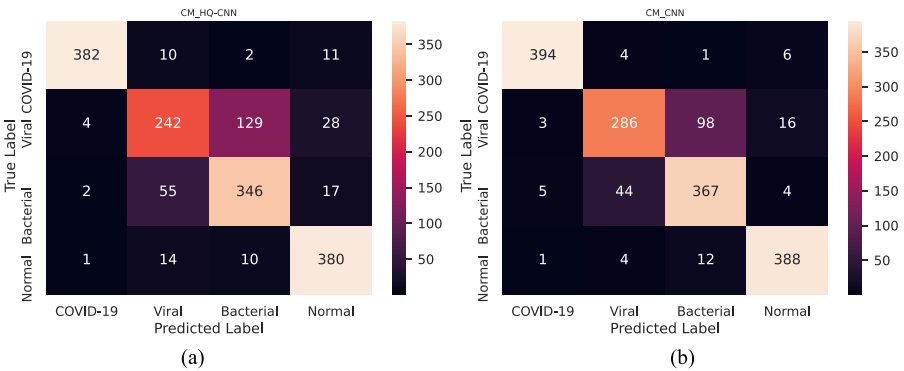


Figure 14: The CM of E4 (a) HQ-CNN and (b) CNN.

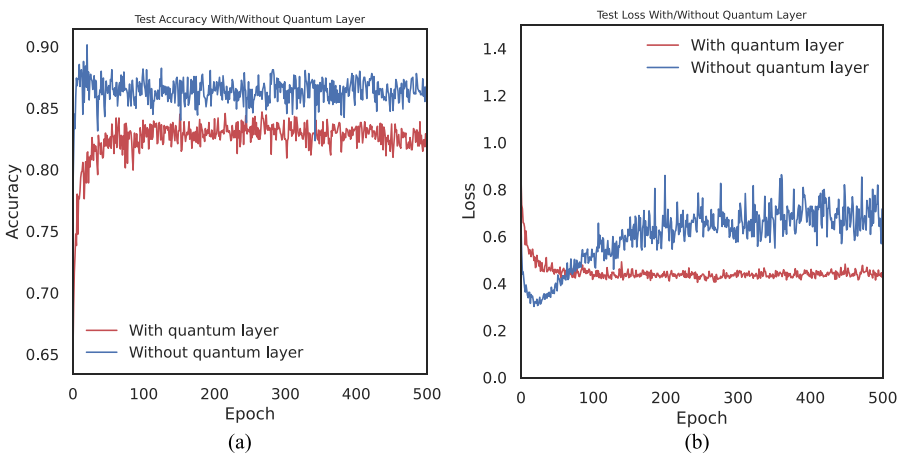


Figure 15: Visualization of the learning curve for both (a) test accuracy and (b) test loss of E4 with 500 epochs.

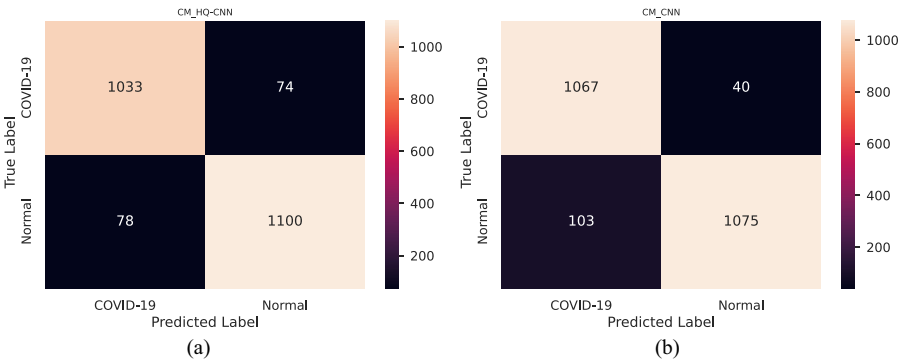


Figure 16: The CM of E5 (a) HQ-CNN and (b) CNN.

and three classical layers). In classical CNN, the quantum layer is replaced by the classical Conv layer with four filters. Most of the state-of-the-art COVID-19 classification is designed to fit the currently limited images as in Oh et al. (2020) and Das et al. (2020) and to help in early diagnosis for COVID-19 cases. Their studies focus on prediction confirmed COVID-19 from COVID-19 and normal datasets such as Ozturk et al. (2020) and other studies focus on differentiating confirmed COVID-19 from other pneumonia diseases (Das et al., 2020; Ezzat et al., 2020; Wu et al., 2020).

The HQ-CNN model has a low number of layers compared to other studies (Das et al., 2020; Ozturk et al., 2020). Besides, the total trainable parameters number of the HQ-CNN model is 119 645 compared to classical CNN (503 665). Also, the proposed model achieved a fewer number of parameters compared to studies in the literature review. From Table 6, with increasing the number of images (E5) or the number of classes (E4), the performance of the proposed model decreases. The HQ-CNN model does not work efficiently with large datasets and multiclass classification.

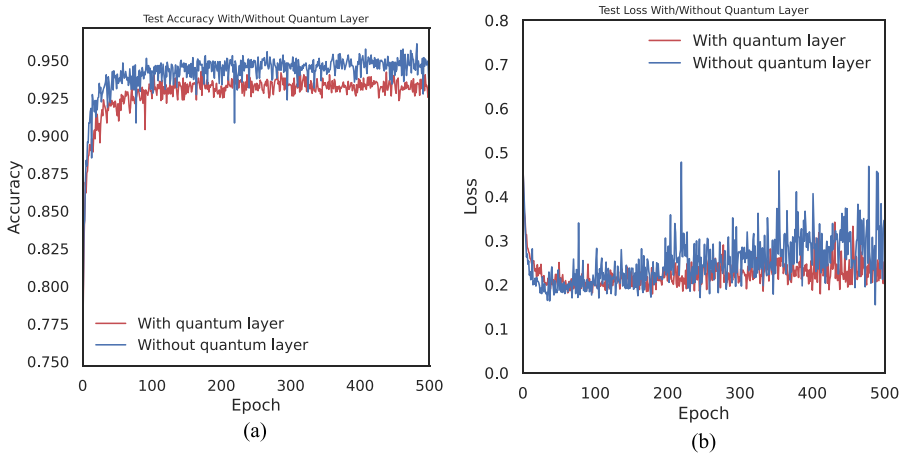


Figure 17: Visualization of the learning curve for both (a) test accuracy and (b) test loss of E5 with 500 epochs.

Table 7: Comparison with CXR existing studies.

Study	COVID-19 images	Class	AC. (%)	Re. (%)	F1-measure(%)
MobileNetV2 (Apostolopoulos & Mpesiana, 2020)	224	multi	96.7	98.66	-
ResNet18 (Oh et al., 2020)	180	multi	88.9	85.9	84.4
Truncated InceptionNet (Das et al., 2020)	162	multi	99.9	98	98
DarkNet (Ozturk et al., 2020)	125	binary	98.08	95.13	96.51
DarkNet (Ozturk et al., 2020)	125	multi	87.02	85.35	87.37
CNN + LSTM (Islam et al., 2020)	1512	binary	99.4	99.3	99.9
CoroNet (Khan et al., 2020)	280	binary	99	99.3	98.5
CoroNet (Khan et al., 2020)	280	multi	95	96.9	95.6
VGG16 (Brunese et al., 2020)	250	binary	96	96	94
GSA-DenseNet121 (Ezzat et al., 2020)	99	binary	98.38	98.5	98
Inception + FO-MPA (Sahlol et al., 2020)	200	binary	98.7	-	98.2
Inception + FO-MPA (Sahlol et al., 2020)	219	binary	99.6	-	99
CapsNet (Toraman et al., 2020)	1050	binary	97.24	97.42	97.24
CapsNet (Toraman et al., 2020)	1050	multi	84.22	84.22	84.21
EfficientNet (Marques et al., 2020)	504	binary	99.62	99.63	99.62
EfficientNet (Marques et al., 2020)	504	multi	96.70	96.69	97.11
HQ-CNN	1350	binary	98.6	99	98.6
HQ-CNN	3616	binary	93.3	93.3	93.5
HQ-CNN	1350	multi	82.2	82.6	88.8

Quantum preprocessing divided the resolution of an image with an input size of $(28 \times 28 \times 1)$ into $(14 \times 14 \times 4)$ and this is compatible with the classical convolution process with a kernel size of (2×2) and stride is equal to 2. The input image is encoding into a quantum circuit, which is accomplished using parametrized rotations performed to the ground state of qubits. On the quantum device, a quantum computation associated with a unitary U is conducted. This unitary can be generated by RQC. Finally, the quantum system is measured to produce measurement findings (classical expectation values). Each expectation value is assigned to one of the four channels of a single output pixel; the same technique is applied to the entire input image to build an output object with a multichannel image. Classical Conv layers are added after the quantum Conv layer

In the statistical analysis, the HQ-CNN model achieved higher values with 98.2% average accuracy, 97.2% Kappa score, and 97.2% MCC in E1. In E2, the HQ-CNN model scored 97.8% average accuracy, 96.5% Kappa score, and 96.5 % MCC. Also, it obtained an average accuracy of 97.9%, 96.1% Kappa score, and MCC in E3. In the multiclass experiment, it scored

82.5%, 76.8%, and 77.1% for average accuracy, Kappa score, and MCC, respectively. The higher values of Kappa score and MCC show higher robustness and better similarity of the HQ-CNN mode

Table 8 shows the results of the HQ-CNN model with each class of E1, E2, E3, E4, and E5. In E1, the COVID-19 class is predicted with high accuracy of 98.6%, recall of 99%, and F1-measure of 99%. In normal cases, The HQ-CNN model obtained 98% recall. In E2, the COVID-19 class is categorized with 99%, 97%, and 98% for recall, precision, and F1-measure, respectively. In viral pneumonia cases, the viral class obtained the higher precision with 100%. Furthermore, in the multiclass experiment (E4), the higher results are obtained with the COVID-19 class. It classified the COVID-19 cases with a recall of 98%, a precision of 94%, and an F1-measure of 96%. Besides, with normal category, it achieved lower results. Figure 18 depicts the results of the HQ-CNN model for E1, E2, E3, and E5 with four images in each experiment. The images entitled in green text describe the images that the HQ-CNN model correctly classified. Meanwhile, the images entitled in the red text represent the samples that the HQ-CNN model incorrectly classified.

Table 8: The HQ-CNN model performance with each class for the five experimental results.

Class	Re. (%)	Pr. (%)	F1-measure (%)
E1			
COVID-19	99	98	99
normal	98	99	99
E2			
COVID-19	99	97	98
viral	97	100	98
E3			
COVID-19	99	97	98
bacterial	97	99	98
E4			
COVID-19	98	94	96
normal	75	60	67
viral	71	82	76
bacterial	87	94	90
E5			
COVID-19	93	93	93
normal	94	93	94

Table 9: Computational time in seconds for the five experimental results.

Model	Training time (s)	Encoding time (s)
E1		
HQ-CNN	456.6	1201
CNN	791.6	-
E2		
HQ-CNN	378	1203
CNN	1042	-
E3		
HQ-CNN	329	1203
CNN	1020	-
E4		
HQ-CNN	1802	2935
CNN	1792	-
E5		
HQ-CNN	2100	3600
CNN	3923	-

Moreover, the training time and encoding time are depicted in Table 9. The training time of the HQ-CNN model needed 456.6, 378, 329, 1802, and 2100s for E1, E2, E3, E4, and E5, respectively. Meanwhile, the training time of the CNN model took 791.6, 1042, 1020, 1792, and 3923s, respectively. This means that the HQ-CNN model took less training time compared with the CNN model. However, the encoding time to encode input images into quantum features required 1200.5, 1203, 1203, 2935, and 3600s for E1, E2, E3, E4, and E5, respectively, as seen in Table 9. The HQ-CNN model is faster than the classical CNN model in training time and other models (i.e., El Asnaoui & Chawki, 2020; Islam et al., 2020). The HQ-CNN model consumed 2100s, CNN took 3923s, the InceptionResNetV2 (El Asnaoui & Chawki, 2020) required 79 184.28s, and CNN + LSTM (Islam et al., 2020) needed 18372s for training time.

The proposed HQ-CNN model has some shortcomings, which are as follows:

1. We use near-term quantum devices as it necessitates small quantum circuits to match the available number of qubits. So, the input images are presented in low dimensions. The quantum kernel introduces some local distortion as well as resolution downsampling. However, the overall contour of the image is preserved and not altered, as would be expected from the classical convolution layer, as shown in Fig. 4.
2. Due to the small architecture of the HQ-CNN model, the HQ-CNN model does not work efficiently with large datasets and multiclass classification [i.e. NIH Chest X-ray dataset (<https://www.kaggle.com/nih-chest-xrays/sample>, <https://www.kaggle.com/nih-chest-xrays/data>) (Wang et al., 2017), and imagenet], so we will work on improving the method and this is part of our future work.
3. Because our model does not go through rigorous clinical validation, we plan to make it available to hospitals so that radiologists can provide feedback.

6. Conclusion and Future Works

Because of QC's superiority and progress, a hybrid of ML and QC is integrated with many fields (e.g. ML and healthcare). In this work, a new HQ-CNN model is proposed for COVID-19 prediction with chest radiography images. The HQ-CNN model has used the RQC as a quantum convolution layer to compute convolution operation on a quantum device. To investigate the performance, the HQ-CNN model is evaluated over many experiments: First, the HQ-CNN model achieved an average accuracy of 98.2%, a Kappa score of 97.2%, and an MCC of 72.2% in experiment 1 (COVID-19 and normal cases). Second, it achieved 97.8%, 96.5%, and 96.5% for an average accuracy, Kappa score, and MCC, respectively, in experiment 2 (COVID-19 and viral pneumonia cases). Third, in experiment 3 (COVID-19 and bacterial pneumonia cases), the HQ-CNN model obtained an average accuracy of 97.9%, a Kappa score of 96.1%, and an MCC of 96.1%. The proposed model's results have been shown to have significant effects on COVID-19 detection using X-ray images. The proposed method could distinguish between COVID-19, viral pneumonia, and bacterial pneumonia, as well as normal cases. Finally, the statistical analysis shows the reliability and validity of the HQ-CNN model and good classification performance.

The limitations of the proposed HQ-CNN model in this work are as follows: The size of the COVID-19 image is used with

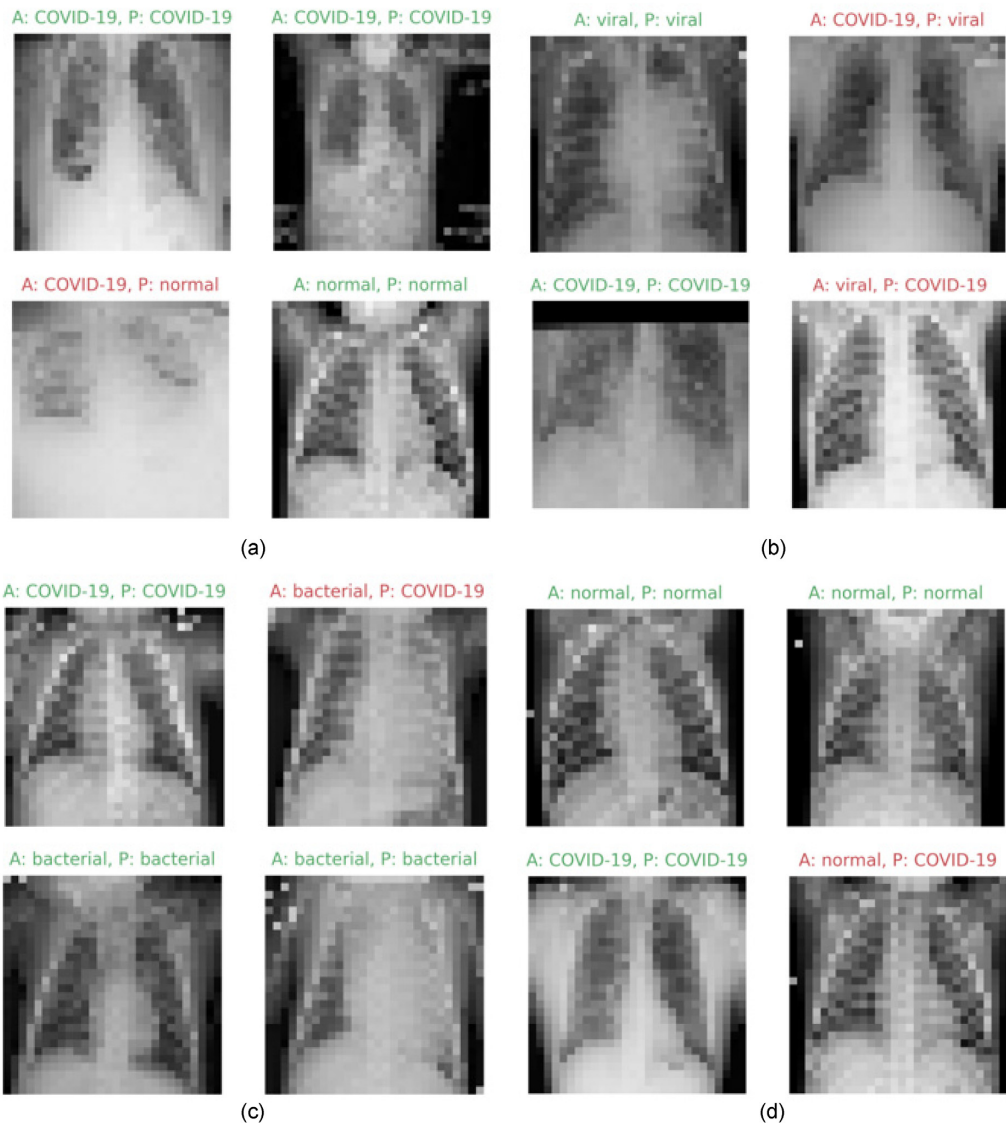


Figure 18: Validation of the HQ-CNN model from sample images on (a) E1, (b) E2, (c) E3, and (d) E5. A represents actual images, and P represents predicted images.

28×28 pixels. The architecture of the HQ-CNN model has a few layers to match small-scale quantum hardware. The HQ-CNN model does not work efficiently with large datasets and multiclass classification (i.e. Imagenet), so we will work on improving the method and this is part of our future work. Because our model does not go through rigorous clinical validation, we plan to make it available to hospitals so that radiologists can provide feedback.

Therefore, the future work will be highly focused on using different encoding methods (i.e. amplitude encoding) with further quantum convolutional layers. Besides, we will use the proposed model on a larger dataset. Finally, we will enhance the HQ-CNN architecture to overcome limitations of the proposed model.

Compliance with ethical standards

This article does not contain any studies with human participants or animals performed by any of the authors.

Acknowledgments

The authors would like to thank Pennylane's team members for helpful discussions, especially Dr. Andrea Mari for valuable discussions. Also, we are grateful to the reviewers for their comprehensive review and appreciate their comments, suggestions, and recommendations, which significantly contributed to improving the paper's quality.

Author contribution statement

Essam H. Houssein: Supervision, Software, Methodology, Conceptualization, Formal analysis, Investigation, Visualization, and Writing – Review and Editing. Zainab Abohashima: Software, Resources, Data Curation, and Writing – Original Draft. Mohamed Elhoseny: Methodology, Conceptualization, Formal analysis, and Writing – Review and Editing. Waleed M. Mohamed: Methodology, Conceptualization, Formal analysis, and Writing – Review and Editing. All authors read and approved the final paper.

Conflict of interest statement

None declared.

Data Availability

All data generated or analysed during this study are included in this published article and are available in Chowdhury et al. (2020) and Kermany et al. (2018).

References

- Abbas, A., Abdelsamea, M. M., & Gaber, M. M. (2021). 4S-DT: Self-supervised super sample decomposition for transfer learning with application to Covid-19 detection. *IEEE Transactions on Neural Networks and Learning Systems*, 32, 2798–2808.
- Abdel-Basset, M., Mohamed, R., Elhoseny, M., Chakrabortty, R. K., & Ryan, M. (2020). A hybrid Covid-19 detection model using an improved marine predators algorithm and a ranking-based diversity reduction strategy. *IEEE Access*, 8, 79521–79540.
- Abualigah, L., Diabat, A., Mirjalili, S., Abd Elaziz, M., & Gandomi, A. H. (2021a). The arithmetic optimization algorithm. *Computer Methods in Applied Mechanics and Engineering*, 376, 113609.
- Abualigah, L., Yousri, D., Abd Elaziz, M., Ewees, A. A., Al-qaness, M. A., & Gandomi, A. H. (2021b). Aquila optimizer: A novel meta-heuristic optimization algorithm. *Computers & Industrial Engineering*, 157, 107250.
- Ahmadianfar, I., Heidari, A. A., Gandomi, A. H., Chu, X., & Chen, H. (2021). Run beyond the metaphor: An efficient optimization algorithm based on Runge Kutta method. *Expert Systems with Applications*, 181, 115079.
- Ahmed, M. M., Houssein, E. H., Hassani, A. E., Taha, A., & Has-sani, E. (2019). Maximizing lifetime of large-scale wireless sensor networks using multi-objective whale optimization algorithm. *Telecommunication Systems*, 72(2), 243–259.
- Ahmed, S. F., Quadeer, A. A., & McKay, M. R. (2020). Preliminary identification of potential vaccine targets for the Covid-19 coronavirus (SARS-CoV-2) based on SARS-CoV immunological studies. *Viruses*, 12(3), 254.
- Aimeur, E., Brassard, G., & Gambs, S. (2006). Machine learning in a quantum world. In *Conference of the Canadian Society for Computational Studies of Intelligence*(pp. 431–442). Springer.
- Al-qaness, M. A., Ewees, A. A., Fan, H., & Abd El Aziz, M. (2020). Optimization method for forecasting confirmed cases of Covid-19 in China. *Journal of Clinical Medicine*, 9(3), 674.
- Amin, J., Sharif, M., Gul, N., Kadry, S., & Chakraborty, C. (2021). Quantum machine learning architecture for Covid-19 classification based on synthetic data generation using conditional adversarial neural network. *Cognitive Computation*, 13, 1–12.
- Apostolopoulos, I. D., & Mpjesiana, T. A. (2020). Covid-19: Automatic detection from X-ray images utilizing transfer learning with convolutional neural networks. *Physical and Engineering Sciences in Medicine*, 43, {635–640}.
- Arute, F. et al. (2019). Quantum supremacy using a programmable superconducting processor. *Nature*, 574(7779), 505–510.
- Bergholm, V., Isaac, J., Schuld, M., Gogolin, C., Blank, C., McKernan, K., & Killoran, N. (2018). PennyLane: Automatic differentiation of hybrid quantum-classical computations. preprint arXiv:1811.04968.
- Boixo, S., Isakov, S. V., Smelyanskiy, V. N., Babbush, R., Ding, N., Jiang, Z., Bremner, M. J., Martinis, J. M., & Neven, H. (2018). Characterizing quantum supremacy in near-term devices. *Nature Physics*, 14(6), 595–600.
- Brunese, L., Mercaldo, F., Reginelli, A., & Santone, A. (2020). Explainable deep learning for pulmonary disease and coronavirus Covid-19 detection from X-rays. *Computer Methods and Programs in Biomedicine*, 196, 105608.
- Chattopadhyay, S., Dey, A., Singh, P. K., Geem, Z. W., & Sarkar, R. (2021). Covid-19 detection by optimizing deep residual features with improved clustering-based golden ratio optimizer. *Diagnostics*, 11(2), 315.
- Chen, N., Zhou, M., Dong, X., Qu, J., Gong, F., Han, Y., Qiu, Y., Wang, J., Liu, Y., Wei, Y., Xia, J., Yu, T., Zhang, X., & Zhang, L. (2020). Epidemiological and clinical characteristics of 99 cases of 2019 novel coronavirus pneumonia in Wuhan, China: A descriptive study. *The Lancet*, 395(10223), 507–513.
- Chicco, D., & Jurman, G. (2020). The advantages of the Matthews correlation coefficient (MCC) over F1 score and accuracy in binary classification evaluation. *BMC Genomics*, 21(1), 1–13.
- Chicco, D., Warrens, M. J., & Jurman, G. (2021). The Matthews correlation coefficient (MCC) is more informative than Cohen's Kappa and Brier score in binary classification assessment. *IEEE Access*, 9, 78368–78381.
- Chowdhury, M. E., Rahman, T., Khandakar, A., Mazhar, R., Kadir, M. A., Mahbub, Z. B., Islam, K. R., Khan, M. S., Iqbal, A., Al-Emadi, N., Bin Ibne Reaz, M., & Islam, M. T. (2020). Can AI help in screening viral and Covid-19 pneumonia? *IEEE Access*, 8, 132665–132676.
- Ciliberto, C., Herbster, M., Ialongo, A. D., Pontil, M., Rocchetto, A., Severini, S., & Wossnig, L. (2018). Quantum machine learning: A classical perspective. *Proceedings of the Royal Society A: Mathematical, Physical and Engineering Sciences*, 474(2209), 20170551.
- Das, D., Santosh, K., & Pal, U. (2020). Truncated inception net: Covid-19 outbreak screening using chest X-rays. *Physical and Engineering Sciences in Medicine*, 43, 1–11.
- Dunjko, V., & Briegel, H. J. (2018). Machine learning & artificial intelligence in the quantum domain: A review of recent progress. *Reports on Progress in Physics*, 81(7), 074001.
- Dunjko, V., Taylor, J. M., & Briegel, H. J. (2016). Quantum-enhanced machine learning. *Physical Review Letters*, 117(13), 130501.
- El Asnaoui, K., & Chawki, Y. (2020). Using X-ray images and deep learning for automated detection of coronavirus disease. *Journal of Biomolecular Structure and Dynamics*, 39, 1–12.
- Ezzat, D., Ella, H. A., & Aboul Ella, H. (2020). An optimized deep learning architecture for the diagnosis of Covid-19 disease based on gravitational search optimization. *Applied Soft Computing Journal*, 98, 106742.
- Farhi, E., & Neven, H. (2018). Classification with quantum neural networks on near term processors. preprint arXiv:1802.06002.
- Gao, D., Wang, G.-G., & Pedrycz, W. (2020). Solving fuzzy job-shop scheduling problem using de algorithm improved by a selection mechanism. *IEEE Transactions on Fuzzy Systems*, 28, 3265–3275.
- Hashim, F. A., Houssein, E. H., Hussain, K., Mabrouk, M. S., & Al-Atabany, W. (2020a). A modified henry gas solubility optimization for solving motif discovery problem. *Neural Computing and Applications*, 32(14), 10759–10771.
- Hashim, F. A., Houssein, E. H., Mabrouk, M. S., Al-Atabany, W., & Mirjalili, S. (2019). Henry gas solubility optimization: A novel physics-based algorithm. *Future Generation Computer Systems*, 101, 646–667.
- Hashim, F. A., Hussain, K., Houssein, E. H., Mabrouk, M. S., & Al-Atabany, W. (2020b). Archimedes optimization algorithm: A

- new metaheuristic algorithm for solving optimization problems. *Applied Intelligence*, 51, 1–21.
- Havlíček, V., Córcoles, A. D., Temme, K., Harrow, A. W., Kandala, A., Chow, J. M., & Gambetta, J. M. (2019). Supervised learning with quantum-enhanced feature spaces. *Nature*, 567(7747), 209–212.
- Hemdan, E. E.-D., Shouman, M. A., & Karar, M. E. (2020). Covidx-net: A framework of deep learning classifiers to diagnose Covid-19 in X-ray images. preprint arXiv:2003.11055.
- Henderson, M., Shakya, S., Pradhan, S., & Cook, T. (2020). Quantum convolutional neural networks: powering image recognition with quantum circuits. *Quantum Machine Intelligence*, 2(1), 1–9.
- Houssein, E. H., Abohashima, Z., Elhoseny, M., & Mohamed , W. M. (2022)Machine learning in the quantum realm: The state-of-the-art, challenges, and future vision. *Expert Systems with Application*.194, 116512.
- Houssein, E. H., Hosney, M. E., Elhoseny, M., Oliva, D., Mohamed, W. M., & Hassaballah, M. (2020a). Hybrid harris hawks optimization with cuckoo search for drug design and discovery in chemoinformatics. *Scientific Reports*, 10(1), 1–22.
- Houssein, E. H., Saad, M. R., Hashim, F. A., Shaban, H., & Hassaballah, M. (2020b). Lévy flight distribution: A new metaheuristic algorithm for solving engineering optimization problems. *Engineering Applications of Artificial Intelligence*, 94, 103731.
- Islam, M. Z., Islam, M. M., & Asraf, A. (2020). A combined deep CNN-LSTM network for the detection of novel coronavirus (Covid-19) using X-ray images. *Informatics in Medicine Unlocked*, 20, 100412.
- Jaiswal, A., Gianchandani, N., Singh, D., Kumar, V., & Kaur, M. (2020). Classification of the Covid-19 infected patients using densenet201 based deep transfer learning. *Journal of Biomolecular Structure and Dynamics*, 39, 1–8.
- Jamil, S., Mark, N., Carlos, G., Cruz, C. S. D., Gross, J. E., & Pasnick, S. (2020). Diagnosis and management of Covid-19 disease. *American Journal of Respiratory and Critical Care Medicine*, 201(10), P19–P20.
- Jeswal, S., & Chakraverty, S. (2019). Recent developments and applications in quantum neural network: A review. *Archives of Computational Methods in Engineering*, 26(4), 793–807.
- Johri, S., Goyal, M., Jain, S., Baranwal, M., Kumar, V., & Upadhyay, R. (2021). A novel machine learning-based analytical framework for automatic detection of Covid-19 using chest X-ray images. *International Journal of Imaging Systems and Technology*, 31(3), 1105–1119.
- Kak, S. C. (1995). Quantum neural computing. In *Advances in imaging and electron physics*(Vol. 94, pp. 259–313). Elsevier.
- Kaye, P., Laflamme, R., & Mosca, M. (2007). *An introduction to quantum computing*. Oxford University Press.
- Kermany, D. S. et al. (2018). Identifying medical diagnoses and treatable diseases by image-based deep learning. *Cell*, 172(5), 1122–1131.
- Khan, A. I., Shah, J. L., & Bhat, M. M. (2020). Coronet: A deep neural network for detection and diagnosis of Covid-19 from chest X-ray images. *Computer Methods and Programs in Biomedicine*, 196, 105581.
- Killoran, N., Bromley, T. R., Arrazola, J. M., Schuld, M., Quesada, N., & Lloyd, S. (2019). Continuous-variable quantum neural networks. *Physical Review Research*, 1(3), 033063.
- Kooraki, S., Hosseini, M., Myers, L., & Gholamrezanezhad, A. (2020). Coronavirus (Covid-19) outbreak: What the department of radiology should know. *Journal of the American College of Radiology*, 17, 447–451.
- LeCun, Y., Boser, B., Denker, J. S., Henderson, D., Howard, R. E., Hubbard, W., & Jackel, L. D. (1989). Backpropagation applied to handwritten zip code recognition. *Neural computation*, 1(4), 541–551.
- Li, X., Zeng, W., Li, X., Chen, H., Shi, L., Li, X., Xiang, H., Cao, Y., Chen, H., & Liu, C. (2020). CT imaging changes of corona virus disease 2019 (Covid-19): A multi-center study in southwest China. *Journal of Translational Medicine*, 18, 1–8.
- Li, Y., & Xia, L. (2020). Coronavirus disease 2019 (Covid-19): Role of chest CT in diagnosis and management. *American Journal of Roentgenology*, 214(6), 1280–1286.
- Li, Z., Dong, M., Wen, S., Hu, X., Zhou, P., & Zeng, Z. (2019). Clu-CNNs: Object detection for medical images. *Neurocomputing*, 350, 53–59.
- Liu, X., Deng, Z., & Yang, Y. (2019). Recent progress in semantic image segmentation. *Artificial Intelligence Review*, 52(2), 1089–1106.
- Lloyd, S., Schuld, M., Ijaz, A., Izaac, J., & Killoran, N. (2020). Quantum embeddings for machine learning. preprint arXiv:2001.03622.
- Lundervold, A. S., & Lundervold, A. (2019). An overview of deep learning in medical imaging focusing on MRI. *Zeitschrift für Medizinische Physik*, 29(2), 102–127.
- Marques, G., Agarwal, D., & de la Torre Díez, I. (2020). Automated medical diagnosis of Covid-19 through EfficientNet convolutional neural network. *Applied Soft Computing*, 96, 106691.
- McHugh, M. L. (2012). Interrater reliability: The Kappa statistic. *Biochimia Medica*, 22(3), 276–282.
- Miller, D. D., & Brown, E. W. (2018). Artificial intelligence in medical practice: The question to the answer? *The American Journal of Medicine*, 131(2), 129–133.
- Mitarai, K., Negoro, M., Kitagawa, M., & Fujii, K. (2018). Quantum circuit learning. *Physical Review A*, 98(3), 032309.
- Naruei, I., & Keynia, F. (2021). Wild horse optimizer: A new meta-heuristic algorithm for solving engineering optimization problems. *Engineering with Computers*, 1–32. <https://doi.org/10.1007/s00366-021-01438-z>.
- Neggaz, N., Houssein, E. H., & Hussain, K. (2020). An efficient henry gas solubility optimization for feature selection. *Expert Systems with Applications*, 152, 113364.
- Nielsen, M. A., & Chuang, I. (2002). Quantum computation and quantum information.
- Oh, Y., Park, S., & Ye, J. C. (2020). Deep learning Covid-19 features on CXR using limited training data sets. *IEEE Transactions on Medical Imaging*, 39, 2688–2700.
- Ozturk, T., Talo, M., Yildirim, E. A., Baloglu, U. B., Yildirim, O., & Acharya, U. R. (2020). Automated detection of Covid-19 cases using deep neural networks with X-ray images. *Computers in Biology and Medicine*, 121, 103792.
- Sahlol, A. T., Yousri, D., Ewees, A. A., Al-Qaness, M. A., Damasevicius, R., & Abd Elaziz, M. (2020). Covid-19 image classification using deep features and fractional-order marine predators algorithm. *Scientific Reports*, 10(1), 1–15.
- Salehi, S., Abedi, A., Balakrishnan, S., & Gholamrezanezhad, A. (2020). Coronavirus disease 2019 (Covid-19): A systematic review of imaging findings in 919 patients. *American Journal of Roentgenology*, 215, 1–7.
- Schuld, M., & Killoran, N. (2019). Quantum machine learning in feature Hilbert spaces. *Physical Review Letters*, 122(4), 040504.
- Singh, D., Kumar, V., & Kaur, M. (2020). Classification of Covid-19 patients from chest CT images using multi-objective differential evolution-based convolutional neural networks. *European Journal of Clinical Microbiology & Infectious Diseases*, 39, 1–11.

- Sise, M. E., Baggett, M. V., Shepard, J.-A. O., Stevens, J. S., & Rhee, E. P. (2020). Case 17-2020: A 68-year-old man with Covid-19 and acute kidney injury. *New England Journal of Medicine*, 382(22), 2147–2156.
- Takeuchi, Y., Morimae, T., & Hayashi, M. (2019). Quantum computational universality of hypergraph states with pauli-x and z basis measurements. *Scientific Reports*, 9(1), 1–14.
- Tang, S., Wang, C., Nie, J., Kumar, N., Zhang, Y., Xiong, Z., & Barnawi, A. (2021). EDL-COVID: Ensemble deep learning for Covid-19 cases detection from chest X-ray images. *IEEE Transactions on Industrial Informatics*, 17, 6539–6549.
- Tavasoli, N., Rezaee, K., Momenzadeh, M., & Sehhati, M. (2021). An ensemble soft weighted gene selection-based approach and cancer classification using modified metaheuristic learning. *Journal of Computational Design and Engineering*, 8(4), 1172–1189.
- Toraman, S., Alakus, T. B., & Turkoglu, I. (2020). Convolutional capsnet: A novel artificial neural network approach to detect Covid-19 disease from X-ray images using capsule networks. *Chaos, Solitons & Fractals*, 140, 110122.
- Ucar, F., & Korkmaz, D. (2020). Covidiagnosis-net: Deep Bayes-SqueezeNet based diagnosis of the coronavirus disease 2019 (Covid-19) from X-ray images. *Medical Hypotheses*, 140, 109761.
- Udugama, B., Kadhireasan, P., Kozlowski, H. N., Malekjahani, A., Osborne, M., Li, V. Y., Chen, H., Mubareka, S., Gubbay, J. B., & Chan, W. C. (2020). Diagnosing Covid-19: The disease and tools for detection. *ACS Nano*, 14(4), 3822–3835.
- Vania, M., & Lee, D. (2021). Intervertebral disc instance segmentation using a multistage optimization mask-RCNN (MOM-RCNN). *Journal of Computational Design and Engineering*, 8(4), 1023–1036.
- Vania, M., Mureja, D., & Lee, D. (2019). Automatic spine segmentation from CT images using convolutional neural network via redundant generation of class labels. *Journal of Computational Design and Engineering*, 6(2), 224–232.
- Vrysis, L., Tsipas, N., Thoidis, I., & Dimoulas, C. (2020). 1D/2D deep CNNs vs. temporal feature integration for general audio classification. *Journal of the Audio Engineering Society*, 68(1/2), 66–77.
- Wang, G.-G., Deb, S., & Cui, Z. (2019). Monarch butterfly optimization. *Neural Computing and Applications*, 31(7), 1995–2014.
- Wang, S.-H., Nayak, D. R., Guttery, D. S., Zhang, X., & Zhang, Y.-D. (2021a). Covid-19 classification by CCSHNet with deep fusion using transfer learning and discriminant correlation analysis. *Information Fusion*, 68, 131–148.
- Wang, S.-H., Zhang, Y., Cheng, X., Zhang, X., & Zhang, Y.-D. (2021b). PSSPNN: Patchshuffle stochastic pooling neural network for an explainable diagnosis of Covid-19 with multiple-way data augmentation. *Computational and Mathematical Methods in Medicine*, 2021, 6633755.
- Wang, X., Peng, Y., Lu, L., Lu, Z., Bagheri, M., & Summers, R. M. (2017). Chestx-ray8: Hospital-scale chest X-ray database and benchmarks on weakly-supervised classification and localization of common thorax diseases. In *Proceedings of the IEEE Conference on Computer Vision and Pattern Recognition*(pp. 2097–2106).
- Wu, X., Hui, H., Niu, M., Li, L., Wang, L., He, B., Yang, X., Li, L., Li, H., Tian, J., & Zha, Y. (2020). Deep learning-based multi-view fusion model for screening 2019 novel coronavirus pneumonia: A multicentre study. *European Journal of Radiology*, 128, 109041.
- Xie, X., Zhong, Z., Zhao, W., Zheng, C., Wang, F., & Liu, J. (2020). Chest CT for typical 2019-nCoV pneumonia: Relationship to negative RT-PCR testing. *Radiology*, 296, 200343.
- Xu, X. et al. (2020). A deep learning system to screen novel coronavirus disease 2019 pneumonia. *Engineering*, 6, 1122–1129.
- Yang, C.-H. H., Qi, J., Chen, S. Y.-C., Chen, P.-Y., Simiscalchi, S. M., Ma, X., & Lee, C.-H. (2021). Decentralizing feature extraction with quantum convolutional neural network for automatic speech recognition. In *ICASSP 2021-2021 IEEE International Conference on Acoustics, Speech and Signal Processing (ICASSP)*(pp. 6523–6527). IEEE.
- Zhang, L., Zhang, L., & Du, B. (2016). Deep learning for remote sensing data: A technical tutorial on the state of the art. *IEEE Geoscience and Remote Sensing Magazine*, 4(2), 22–40.
- Zhang, Y., Wang, G.-G., Li, K., Yeh, W.-C., Jian, M., & Dong, J. (2020). Enhancing MOEA/D with information feedback models for large-scale many-objective optimization. *Information Sciences*, 522, 1–16.